MOMENT CALCULATIONS FOR LOW ENERGY IONS IN JUPITER'S MAGNETOTAIL FROM NASA'S NEW HORIZONS MISSION

by

DEBRUP HUI

Presented to the Faculty of the Graduate School of

The University of Texas at Arlington in Partial Fulfillment

of the Requirements

for the Degree of

MASTER OF SCIENCE IN PHYSICS

THE UNIVERSITY OF TEXAS AT ARLINGTON

August 2009

ACKNOWLEDGEMENTS

After working for last two years on my research, it is time to look back and thank the people without whose help it was difficult to come up with this thesis. My outmost thanks go to my advisor Dr. Yi-Jiun Su, who actually defined and gave dimensions to this work. She introduced me to this work and trained me from the scratch. In spite of my learning curve being slow, she was always there with immense patience and resources. Even after she joined Air Force Research Laboratory she never let me feel her absence. She worked day and night with me at her residence at Boston during this thesis writing. Her all these efforts helped me come out with this thesis today. Thank you Yi-Jiun.

Another person without whom I could not have completed this work is Dr. Sam Jones, who was always there to explain things in the simplest of ways and to help me with IDL programming. I also thank our previous HOD late Prof. Jim Horwitz, who is not with us today to read this thesis but, who always supported and inspired me until his last days. I thank Prof. Dr. Alex Weiss, interim chair, for his continued support after Jim. My thanks goes to all my colleagues in the space physics groups esp., Elizabeth Mitchell, Robert Bruntz, Ximena Cid, Jorge Landivar and Fajer Jaafari for discussing different research related things from time to time.

I extend my heartfelt thanks to Dr. Fran Begenal from University of Colorado at Boulder for her discussions and suggestions with us during this research. I also thank Dr. Heather A. Elliott from Southwest Research Institute, San Antonio, TX, who helped my advisor in starting this work. My thanks go to Dr. D.J McComas, Principal Investigator of the SWAP instrument and Dr. F.J. Crary from the same institute for sharing scientific information regarding the instrument and the data.

I also thank professors Dr. Ramon Lopez and Dr. Manfred Cuntz for taking interest in my research and for taking time to serve in my thesis committee. Dr. Lopez was always there, silently, to boost my confidence whenever I felt bit low. I take this opportunity to thank my mathematics teacher Prof. Dr. Zdzislaw Musielak for going through my thesis and his comments in spite of his busy engagements with NASA. My work would not have been so smooth unless people in the physics office were working behind the scene arranging all my administrative works and travelling from time to time. Thank you Margie, Stacy, Fran and Victor.

Lastly, I will thank my family and friends back in India who always kept my moral high and inspired me to work harder towards my goal.

July 23, 2009

ABSTRACT

MOMENT CALCULATIONS FOR LOW ENERGY IONS IN JUPITER'S MAGNETOTAIL FROM NASA'S NEW HORIZONS MISSION

Debrup Hui, M.S.

The University of Texas at Arlington, 2009

Supervising Professor: Yi-Jiun Su

Jupiter's magnetosphere and magnetotail is the largest cohesive structure in our solar system which extends to the orbit of Saturn. One of NASA's objectives is to understand how universal bodies interact with its surroundings. The New Horizons (NH) mission is the first satellite to traverse axially through the Jovian magnetotail and obtain in-situ data. The Solar Wind Around Pluto (SWAP) instrument onboard NH measured low energy ions from 35eV to 7.5 keV in the Jovian magnetotail during its fly-by. We analyzed SWAP data from 500-1750 Jovian radii (R_J) when the spacecraft was spinning. A 3D phase-space density fitting procedure was constructed to calculate fluid moments, such as densities, velocities, The Mach number and densities from which thermal pressure can be determined to better understand the ion characteristics in the magnetotail. The results indicate that Jupiter's magnetotail is a highly dynamic region with tremendous variations.

TABLE OF CONTENTS

LIST OF ILLUSTRATIONS

Figure Page

LIST OF TABLES

LIST OF ABBREVIATIONS

UT=Universal Time=GMT

R_J = Jovian Radius or Jupiter's radius = 71,492km

eV = electron Volt

nPa = nanoPascal=10^{-9} Pascal

psd = phase space density

nT = nano Tesla =10^{-9} Tesla

k = Boltzmann Constant

E/q = Energy per unit charge

SWAP= Solar Wind Around Pluto

NH= New Horizons

DOY =Day Of the Year

FWHM = Full Width at Half Maximum

SwRI= Southwest Research Institute

NASA= National Aeronautical and Space Administration

CHAPTER 1

INTRODUCTION

This thesis is an approach to understand different characteristics of charged particles in Jupiter's magnetotail. Most of the planets in the solar system have an internal dynamo creating a magnetic field. This magnetic field shields the planet by deflecting energetic particles in the solar wind. It forms a cocoon like structure filled with plasmas both from the planet and solar wind. This is called a magnetosphere. Standing against the solar wind, the magnetosphere is elongated in the anti-sunward direction and compressed in the sun-facing side just like a comet. The stretched tail of this magnetosphere is called a

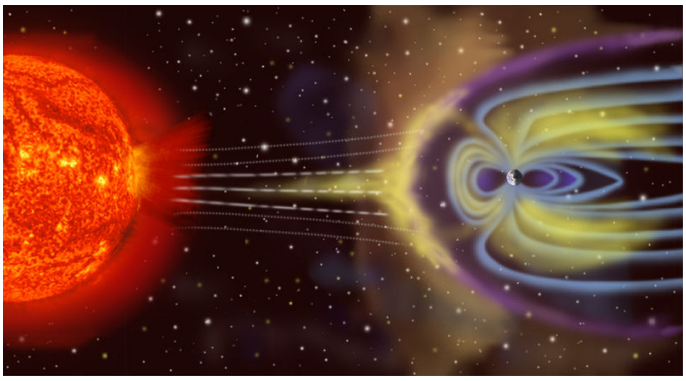

Fig. 1.1: A Magnetosphere is a result of interaction of the solar wind with the magnetic field of a planet. Image credit: NASA

magnetotail. It is formed as a direct consequence of momentum transfer between the magnetosphere and the solar wind. An illustration of the solar wind-magnetosphere interaction is presented in Figure 1.1. The Jovian magnetotail was first reported by Ness et al. [1979a, b, c] when Voyager 1 and Voyager 2 explored the dawn region of the magnetotail at ~100R_J in 1979. The structure and dynamics of the magnetotail is determined by the viscous interaction and the solar wind momentum entry [Khurana et al., 2004]. The Jovian magnetotail is believed to extend

beyond the orbit of Saturn. In fact, Jupiter's magnetosphere is the largest cohesive structure in the solar system. It is so huge that it could encompass the Sun [Russel, 1993].

1.1 Present Understanding

1.1.1 Jupiter's magnetic field and the magnetosphere

It is widely accepted that the core of Jupiter consists of rocks covered with hydrogen under huge pressure from the overlaying layers. This tremendous pressure provides a metallic form to the hydrogen [Space study board, 1994]. Eddy currents in this conducting metallic hydrogen are believed to drive a dynamo process within Jupiter and create its gigantic magnetic field. Jupiter's broad magnetic field is 14 times stronger than the Earth's ranging from 4.2 gauss (0.42 μT) at the equator to 10–14 gauss (1.0–1.4 μT) at the poles, making it the strongest in the solar system (with the exception of sunspots) [Gierasch, and Nicholson, 2004]. Jupiter's dominant magnetic north pole tilts ~11^{o} from its geographic north pole, so the magnetic field comes out of the north pole and goes into the south; hence, the magnetic moment of Jupiter is in the opposite direction from that of the Earth. Unlike the Earth, Jupiter's magnetic field has a strong quadruple component. This component affects the shape and structure of Jupiter's magnetic fields.

The magnetic field deflects the ionized particles in the solar wind around the planet and prevents entering the atmosphere directly. A small part of this ionized plasma enters through open field lines and mixes with atmospheric plasma to form Jupiter's magnetosphere. The boundary where the solar wind meets the planet's magnetosphere is called the magnetopause. Jupiter's magnetopause lies somewhere around 45 to 100 R_J [Khurana et al, 2004] and varies with the solar wind magnetic pressure and solar activity [Russell, 2001]. The bow shock, a wake like disturbance formed by the super-Alfvénic flow overtaking the sub-Alfvénic flow, is located in front of the magnetopause against the solar wind at ~84 R_J [Krupp et al., 2004a]. The magnetosheath is the region between bow shock and the magnetopause.

In the anti-sunward direction, the solar wind pushes field lines to form a long trailing magnetotail, which sometimes extends beyond Saturn's orbit [Grzedzielski et al., 1981]. Jupiter's magnetotail consists of two lobes, with the magnetic field in the northern lobe pointing away from Jupiter and the southern pointing towards the planet. These lobes are separated by a thin plasma layer called the tail current sheet. The magnetotail serves as a channel through which solar plasmas may enter the inner magnetosphere, just like the Earth. When particles are energized and/or heated at around 10 R_J, they form the radiation belts [Khurana et al., 2004]. An illustration of Jupiter's magnetosphere is presented in Figure 1.2.

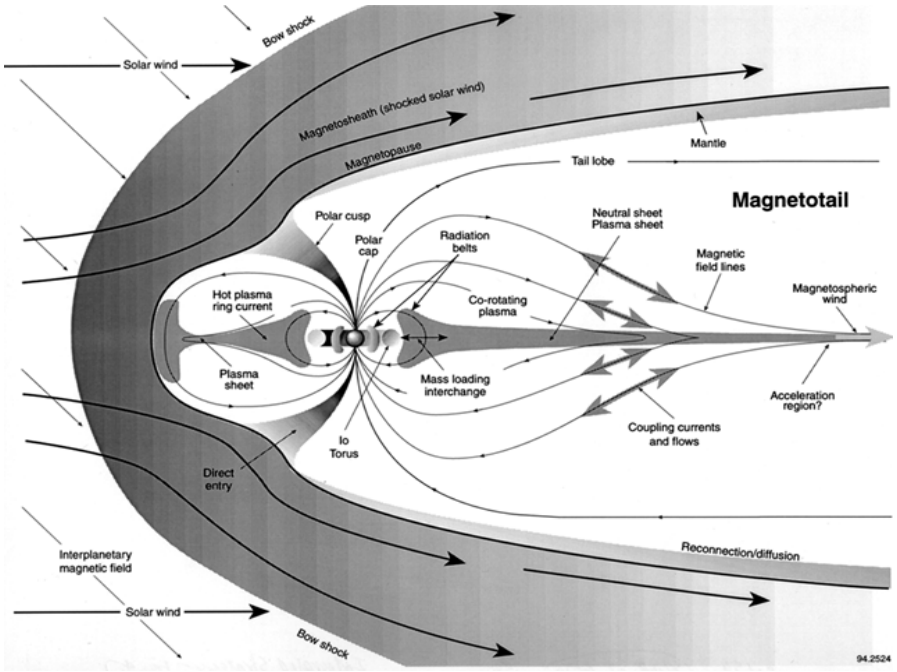

Fig. 1.2: An illustration of Jupiter's magnetosphere and magnetotail.
(Image credit: NASA)

Conventionally, up to 10 R_J is considered as the inner magnetosphere where the field is approximately dipolar. 10-40 R_J is considered as middle and beyond 40 R_J is the outer magnetosphere [Khurana et al., 2004]. 20-40 R_J is sometime referred as the middle magnetosphere [Woch et al., 1998]. In the middle and outer magnetospheres, the fields have

higher magnetic moments which are seriously disturbed by the interaction with the plasmasheet [Khurana et al., 2004]. Very little is known for the outer magnetosphere beyond 200 R_J. Scarf [1979], Kurth et al. [1981], and Lepping et al. [1982] estimated the existence of Jovian magnetotail up to 6,000-9,000 R_J based on Voyager 2 observations.

Jupiter's magnetosphere is a powerful radio source which is much stronger than the Earth's magnetosphere. Electrons within the magnetosphere generate a strong radio signature that produces bursts in the range of ~2-39 MHz. Such radio emissions reach the earth in the form of whistler waves, chorus, and hiss. A full list of Jupiter's emission in different spectra can be found in Bhardwaj and Gladstone [2000].

1.1.2 Sources of Jupiter's Magnetospheric Plasmas

Two major sources of plasmas in the Jovian magnetosphere and magnetotail, other than the solar wind which contributes 100kg s^{-1} [Hill et al., 1983], are: its moon Io and hydrogen rich atmosphere. Jupiter's moon, Io, spews out volcanic gases, roughly 1000 kg s^{-1} mostly sulfur dioxide. Under the UV rays from the Sun, neutral particles are ionized into O^+, S^+, O^{++} and S^{++} and trapped in the planet's strong magnetic field, forming the Io torus [Khurana et al., 2004; Krupp et al., 2004a]. Around 50% of the torus ions are lost via charge exchange; the other half are transported radially outward and ultimately escape down the tail [McComas et al., 2007]. In addition, Jupiter's ionosphere provides almost equal amount of light ions, primarily H^+ and H_3^+, to the magnetosphere. Hot plasmas of ~10eV or above cannot be held by the gravity of Jupiter [Khurana et al., 2004]. Hill et al. [1983] suggested the ionospheric source of plasmas of 20kg s^{-1}. The other comparatively small sources of the Jovian magnetospheric plasmas are the surface sputtering from three icy satellites contributing about 20kg s^{-1} [Khurana et al., 2004; Cooper et al., 2001]. This mixture of ions, along with Jupiter's fast rotation rate (~10 hours),

creates a dense rotating plasma disk that dominates the inner magnetosphere [McComas et al., 2007].

The plasma disk corotates with the planet. Plasmas escape outward to the tail region because of diffusion and interchange instability [Krupp et al., 2004a]. The plasma density reduces from 2,000 cm^{-3} in the torus region to 0.2 cm^{-3} at a distance of 35 R_J. At around 20 R_J in the middle magnetosphere, the corotation gradually breaks and the plasmas outside start slowing down from the corotation [Khurana et al., 2004]. At distances greater than 40 R_J, these plasmas escape the magnetic field completely and leave the magnetosphere through the magnetotail [Russel et al., 2001].

1.1.3 Previous Studies of Jupiter's Magnetosphere

In the modern era of space exploration, 6 fly-by spacecraft and one orbiter satellite have studied the Jovian system. Of all the missions, only Galileo traveled up to 200 R_J into the deep-tail region (inside the magnetotail).

As interesting facts were revealed from the missions, many models of Jupiter's magnetosphere were proposed based on the observations. Goldstein et al. [1985] discussed properties of magnetic fields from 75 R_J to 7500 R_J, where the field lines in the northern and the southern lobes are slightly twisted in the distant tail. The lobes are depleted of plasmas and the density may be as low as ~10^{-2} cm^{-3} at distances greater than 7000 R_J [Blanc et al., 2005]. At around 7000 R_J, the solar wind diffuses into the magnetotail and makes it very turbulent. Behannon et al. [1981] were the first to report the near tail current sheet at 200-300R_J. Lepping et al. [1981] observed that the density of the core region falls to ~10^{-3} cm^{-3} where the magnetic

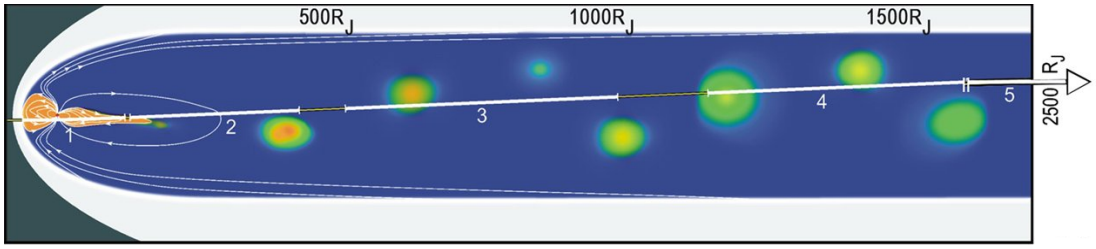

Fig.1.3: A schematic of NH fly by though Jovian magnetotail
(after McComas et al., 2007)

field is minimum in the magnetotail. Kruth et al. [1982] and Grzedzielski and Macek [1984] provided plasma density estimations of 2-3x10^{-2} cm^{-3} at 3-4 AU (~5000R_J) based on their models. Using Cassini data, Krupp et al. [2004b] discussed the energetic particles (electrons above 15keV and ions above 30keV) within the range of 205-800 R_J when the spacecraft was skimming along the bow shock boundary in the dusk to midnight sector. Woch et al. [1998] observed a quasi-periodic 3-day modulation in the ion intensity at 20-80 R_J superimposed over 10 hours rotational periodicity which reappears in the deep tail. However, no spacecraft actually went through the magnetotail providing in-situ data before 2007. New Horizons for the first time made a fly-by almost axially through the Jovian magnetotail (see Figure 1.3) and obtained in-situ charge particle measurements on its way to Pluto. Sittler et al. [1987], Kurth et al. [1982], Goldstein et al. [1985] believed that Voyage 2 crossed the distant tail of Jovian magnetosphere at around 5000-9000 R_J.

1.2 The New Horizons Mission

In some cases, magnetic fields shield surfaces from energetic particles very effectively, conceivably accommodating (or preventing) the evolution of life. Energetic charged particles have been known to destroy instruments onboard manmade satellites and are dangerous to astronauts. Our increasing dependence on satellites to perform tasks vital for everyday life necessitates a understanding of the characteristics of charged particles in space. NASA has

categorized the understanding of how different universal bodies interact with their local environment as one of their primary goals. The New Horizons (NH) mission provides just such an opportunity with *in-situ* observations of Jupiter's interaction with the solar environment in a way never before seen.

NH is one of NASA's deep space missions and the first Pluto mission. It was launched on January 19, 2006. Jupiter provided the gravity assistance for NH in Feburary 2007 to shorten its journey to Pluto by almost two years. Its nearest encounter with Pluto is estimated to be around July 2015. The NH's journey to Pluto is illustrated in Figure 1.4.

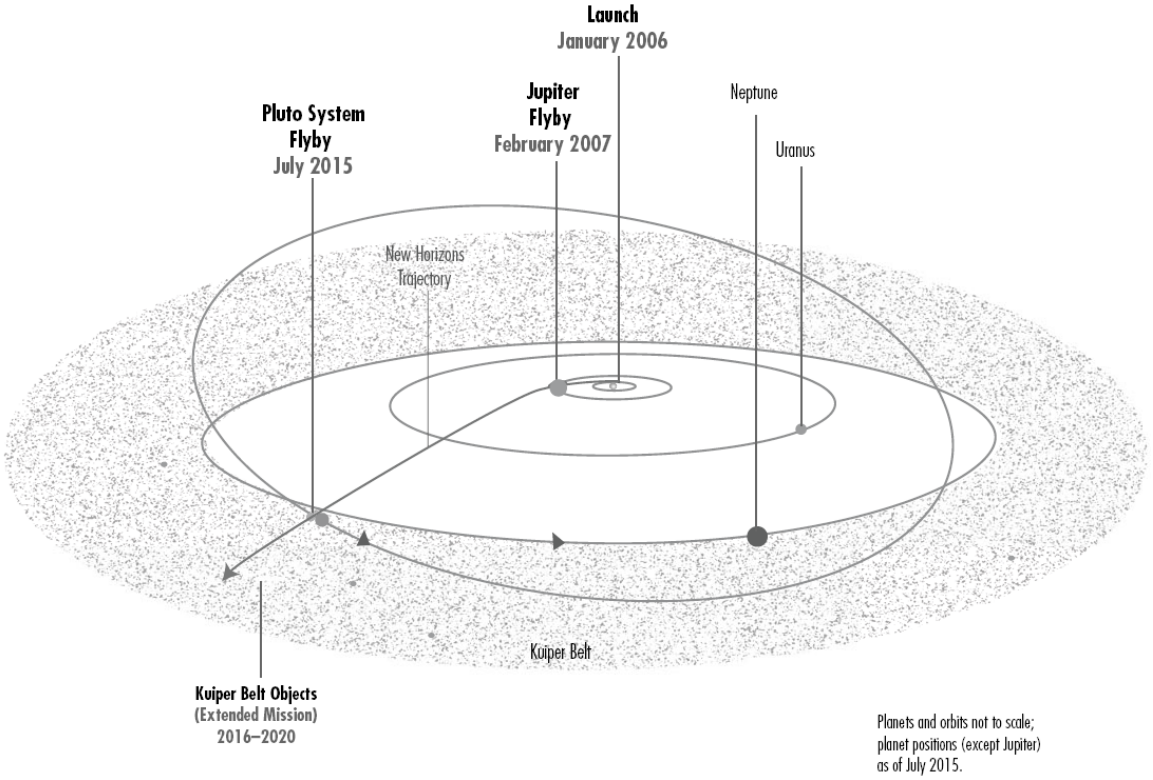

Fig.1.4: NH journey to Pluto (after NH Launch press kit by Brown et al., 2005; 2007)

New Horizons' objectives are (1) to conduct a five-month-long study of the Pluto system as it approaches, flies past (closest approach on 14 July, 1015), and recedes from its target; (2)

to study the global geology and geomorphology of Pluto and Charon, map their surface compositions and temperatures, and examine Pluto's atmospheric composition and structure; (3) to investigate two small moons recently discovered in orbit around Pluto. New Horizons will then head deeper into the Kuiper Belt to investigate one or more of the icy mini-worlds in this vast region, at least a billion miles beyond Neptune's orbit [New Horizons press kit, Brown et al., 2005].

After taking off on 19 January, 2006, NH reached the Jupiter system on 27 February, 2007 soon after which the engineering team switched on the instruments onboard with a reduced sensitivity (as the instruments were build to work at Pluto where solar radiation is much weaker). The spacecraft started spinning on 23 March 2007 at 5 rotations per minute (rpm) and traveled almost axially through Jupiter's magnetotail sampling between 500 and 2500 R_J till 17 June after which the instruments were again put in the hibernation mode [NH Jupiter fly-by press kit; Brown et al., 2007]. More detailed news and updates on the NH mission and Jupiter flyby can be found in Stern et al. [2008], Fountain et al. [2008], Guo and Farquhar [2008] and are available at the following websites: http://pluto.jhuapl.edu, http://www.nasa.gov/newhorizons, and http://www.boulder.swri.edu/pkb

1.3 Instrumentation of New Horizons

The NH spacecraft houses 7 scientific instruments along with a high gain antenna to send back data to the Earth (illustrated in Figure 1.5). It is geared with 16 small hydrazine-propellant thrusters and will obtain most of its energy from the onboard radio-isotope thermal generator at Pluto where solar radiation will not be sufficient enough to generate enough power to run it. More elaborate descriptions can be found in documents such as the New Horizon Jupiter fly-by press kit [Brown et al., 2007], Fountain et al. [2008], Guo and Farquhar [2008], and instrumentation papers given below.

The scientific payload consists of three optical instruments, two plasma instruments, a dust sensor and a radio science receiver/radiometer [NH Launch Press Kit by Brown et al., 2005] as briefly shown below:

(1) **Alice** is a sensitive ultraviolet imaging spectrometer designed to probe the composition and structure of Pluto, Charon, and Kuper Belt Objects (KBOs) [Stern et al., 2008].

(2) **Ralph** is used to study surface geology and morphology of Pluto, its moons and KBOs, and to obtain surface composition and temperature maps of these bodies [Reuter et al., 2008].

(3) **REX** (Radio Science Experiment) measures Pluto's atmospheric temperature and pressure (down to the surface), measures density of the ionosphere, and searches for an atmosphere around Charon [Tyler et al., 2008].

(4) **LORRI** (Long Range Reconnaissance Imager) studies the geology of Pluto, its moons and KBOs, and provides high resolution approach and highest-resolution encounter images of these bodies [Cheng et al., 2008].

(5) **SWAP** (Solar Wind Around Pluto) studies solar wind interactions with Pluto and escape rates of Pluto's atmosphere. It detects low energy particles in its vicinity and their interactions. We describe this instrument in more detail in the next section [McComas et al., 2008].

(6) **PEPSSI** (Pluto Energetic Particle Spectrometer Science Investigation) studies the density, composition, and nature of energetic particles and plasmas resulting from the escape of Pluto's atmosphere [McNutt et al., 2008].

(7) **VB-SDC** (Venetia Burney Student Dust Counter) measures concentration of dust particles in outer solar systems [Horanyi et al., 2008].

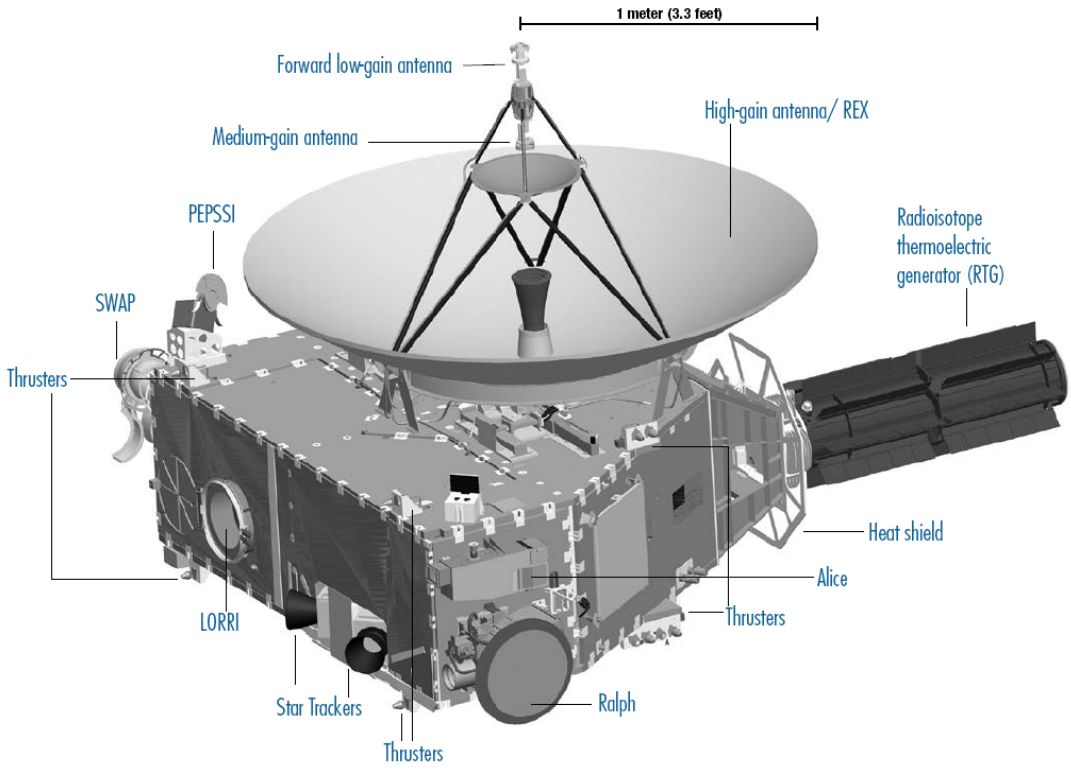

Fig.1.5: NH instrument orientation (from HN press kit by Brown et al., 2005; 2007)

1.3 Solar Wind Around Pluto

The SWAP instrument makes coincidence measurements of ions with energy per charge (E/q) ranging from 35 *eV/q* to 7.5 *keV/q* within a 276^{o} x 10^{o} field-of-view (FOV) centered on NH's high-gain antenna pointing back toward the Earth. SWAP is mounted on the –Zsc side of the spacecraft and the normal to the center of the aperture is aligned with +Ysc (see Figure 1.6b). When the NH spacecraft began spinning at 5 rotations per minute (rpm), SWAP samples ~87% of 4π *sr* excluding a 42^{o} half-angle hole along the anti-sunward spin direction.

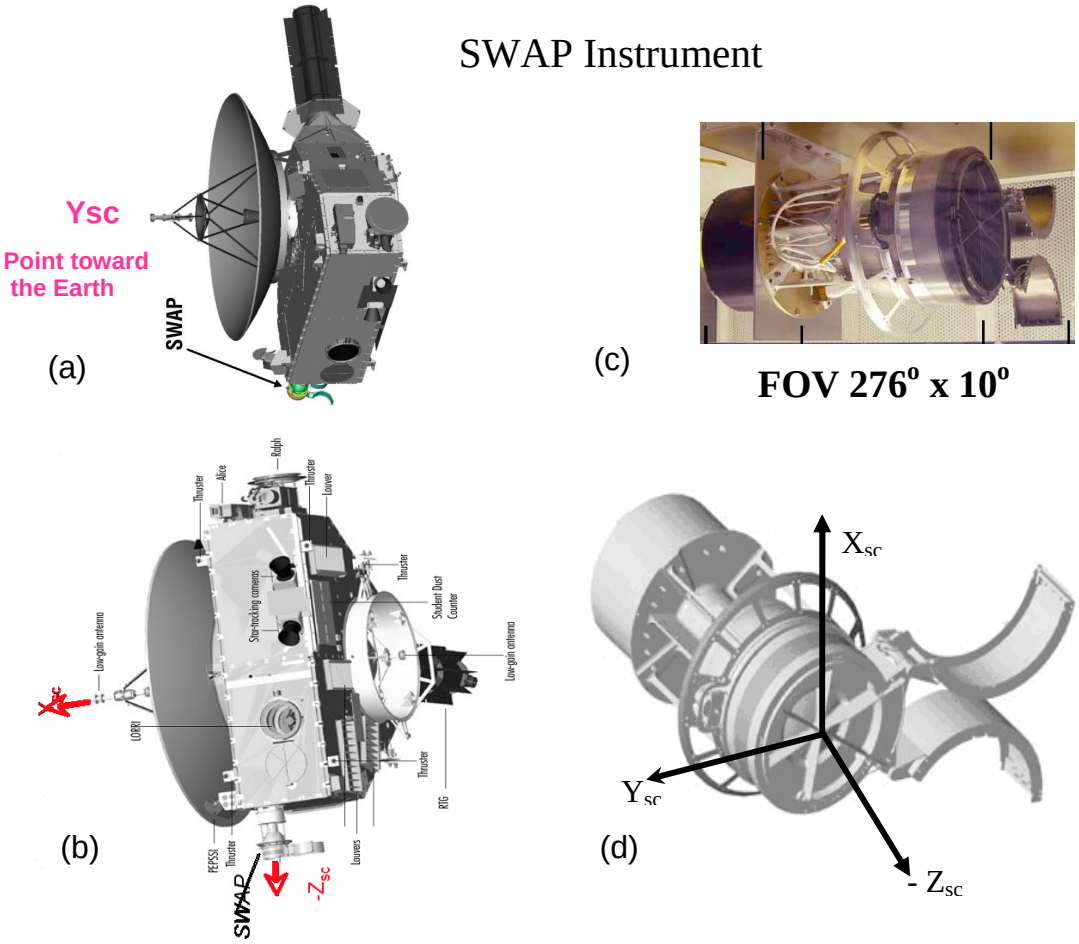

Fig. 1.6: Panels (a) and (b) show the orientation of SWAP on the NH spacecraft. Panels (c) and (d) show the SWAP instrument and its co-ordinate system used for our model (after McComas et al, 2008)

The SWAP instrument is an electrostatic instrument. The electro-optics control the energy band passes of ions entering the instrument. The electro-optics includes the Retarding Potential Analyzer (RPA), the Electrostatic Analyzer (ESA), and the deflector (DFL). These three elements collectively decide which energy band and from which angle solar wind particles or pick up ions can enter the instrument. They are then recognized by a coincidence detector

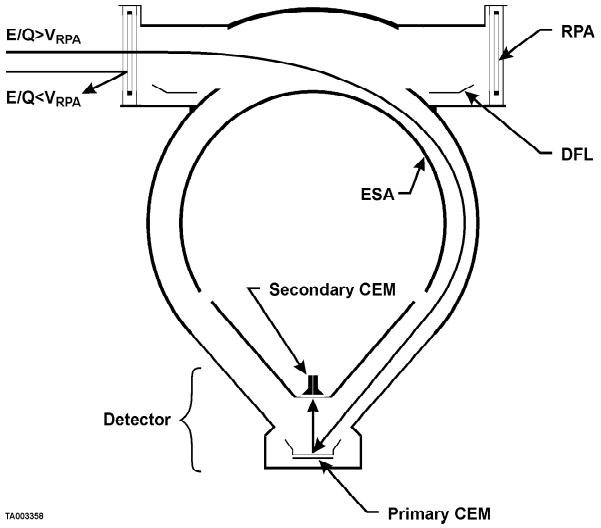

Fig. 1.7: Diagram of SWAP electro-optics. Two ion trajectories are drawn: one having energy greater than the RPA voltage and the other less. [McComas et al., 2008]

system. Figure 1.7 shows a cross section of the instrument. Only ions with E/q greater than RPA voltage are allowed by the high-pass filter. The RPA consists of four grids with the inner two having a positive voltage, which repels ions with energies less than the corresponding potential energy (qV) (top two panels of Figure 1.6). The ESA consists of an inner dome and an outer spherical shell (at ground potential) with a concentric space between the two. Only ions with a limited range of energies pass through the ESA to reach the detector. The deflector is used to adjust FOV. If the solar wind, which is highly collimated (spanning only a few degrees), enters at the bottom of the RPA, the voltage on the deflector could be set so that only ions which are not part of the solar wind beam enter the instrument. This would allow pickup ions, occurring over a wide range of angles, to be studied.

A combination of these 3 elements allows SWAP to make high resolution measurements. It should be noted that during the Jupiter flyby RPA and the deflector were not used. The instrument, while spinning 360^0 in 24 steps makes an energy sweep in 32 energy steps. Each

energy channel is swept over 64 seconds taking 24x64=786 sec for a complete revolution. A detailed description of the instrumentation can be found in *McComas et al.* [2008].

This thesis focuses on analysis of New Horizons data collected during its Jupiter fly-by. We use level 2 scientific data provided by the Southwest Research Institute (SwRI) for our investigation. The second chapter describes the data analysis methodology and the fitting procedure for the moments' calculation. We discuss the data selection criterion between 500 and 1750 R_J and explain various input parameters for the fitting routine based on selected data. A description of the mathematical model used in this thesis is presented in Section 2.2. In Chapter 3, results are discussed in different time scales of a day and longer depending upon the requirements to bring out various features of ion characteristics from SWAP. Chapter 3 contains plots for our analysis, observations, and possible explanations. The analysis technique for both single and double ion species is also provided. Finally, the last chapter summarizes our results with discussions and conclusions.

CHAPTER 2

METHODOLOGY

Mankind's quest to understand the largest cohesive structure in the solar system, Jupiter's magnetotail, was further enhanced when NASA's New Horizon satellite traversed the gigantic magnetotail exceeding 2500 Jovian radii (R_J). An analysis of the data from SWAP, an onboard instrument making coincident measurements of ions, shows that the magnetotail consists of multiple species of light and heavy ions with large density variations. Different periodic structures have also been observed in the magnetotail of Jupiter [*McComas et al.,* 2007]. In order to further our understanding of the physical processes governing the density variation, we have developed a 3-dimensional phase-space distribution fitting procedure to study the characteristics of ions. This procedure is designed to construct the observed signatures along with the calibration parameters provided by the SWAP team during the NH Jupiter's magnetotail flyby. The model requires information of the satellite orientation. This chapter begins with a description of data selection including various input parameters for the model.

2.1 Data Selection

The level 2 scientific data used here are provided by the SWAP team at SwRI. Data are collected during the entire Jupiter fly-by. The energy spectrogram of Jupiter's magnetotail, adopted from McComas et al. [2007], is displayed in Figure 2.1. In this thesis, we only used data shown in panels labeled 3 and 4 in Figure 2.1 (i.e., between ~500 and 1750 R_J on DOYs 82-132) when the spacecraft was spinning before the solar wind entry on DOY 132.

The spacecraft coordinate system is defined in Figure 2.2, where the y-axis (Y_{sc}) is along the spin axis of the satellite. The SWAP instrument is mounted on the negative z direction of the spacecraft ($-Z_{sc}$), while the normal to the center of the aperture is aligned with $+Y_{sc}$. The

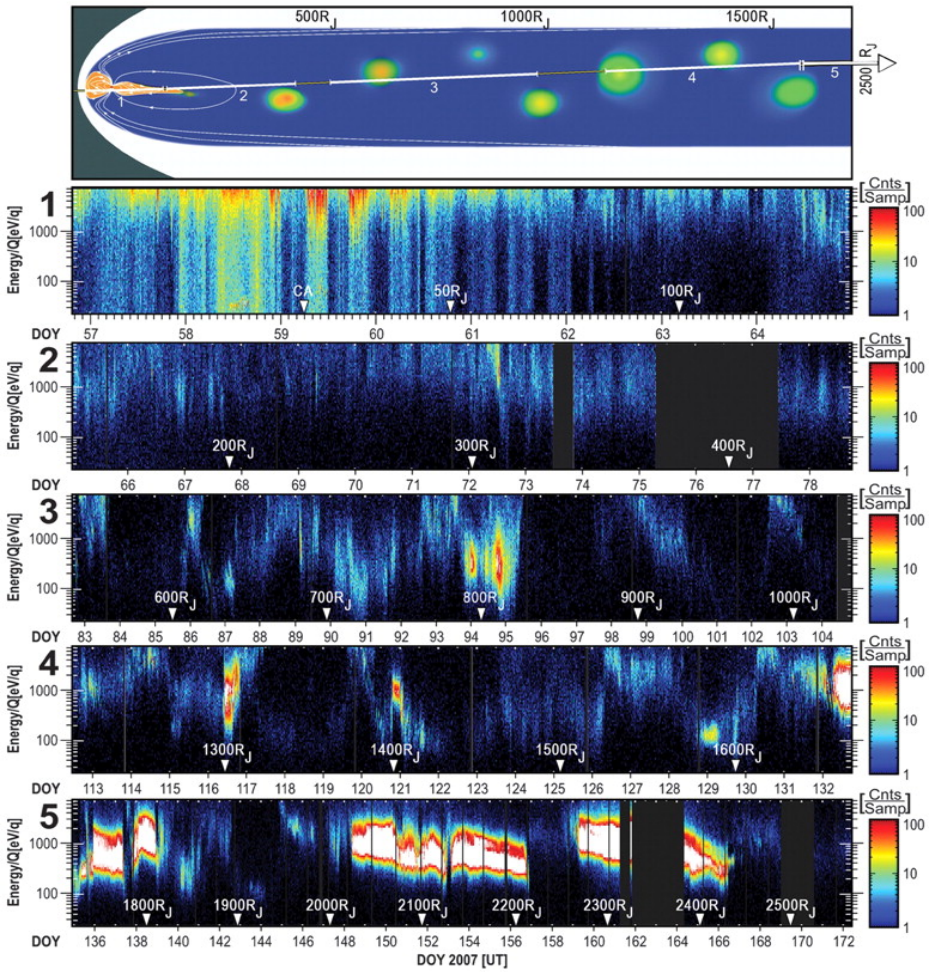

Fig. 2.1: A schematic diagram of a meridional cut through Jupiter's magnetotail (top) shows the stretched plasma current sheet and large plasmoids moving down the tail. The five E/q spectrograms of the log of coincidence count rates per 0.5-s sample cover the five intervals numbered in the schematic. [*McComas et al.*, 2007].

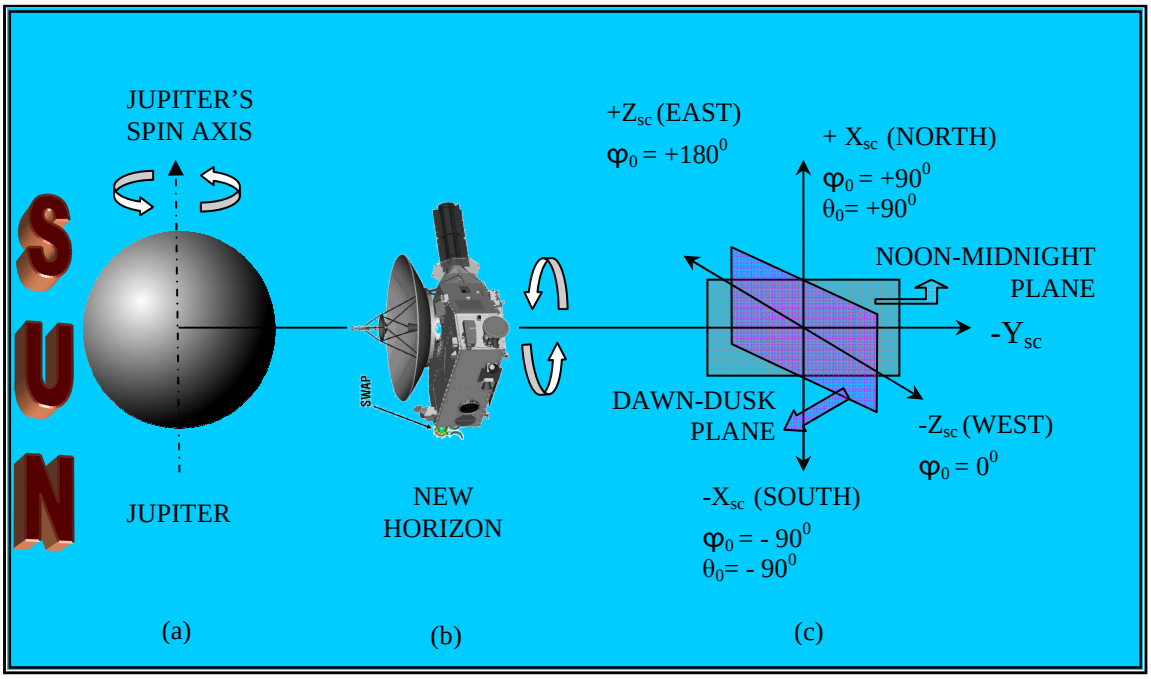

Fig. 2.2: (a) Jupiter with the spin axis pointing north. (b) The NH spacecraft with a spin axis in the sunward direction. The SWAP instrument is mounted at the bottom of the middle panel along the $-Z_{sc}$ axis (see also Figure 2.3). (c) The spacecraft coordinate system.

left panel of Figure 2.3 displays the SWAP instrument with the labeled spacecraft axes. The ion velocity is, hence, obtained in the spacecraft reference frame. Ion velocities are much higher than the speed of spacecraft (~10 $km\ s^{-1}$); therefore, the spacecraft can be treated as a stationary object relative to ion beams. An incoming ion beam in the spacecraft coordinate system is plotted in the right panel of Figure 2.3, where θ_o is defined as the angle between the flow direction and $+Y_{sc}$, and the spacecraft spin angle is labeled as φ_o.

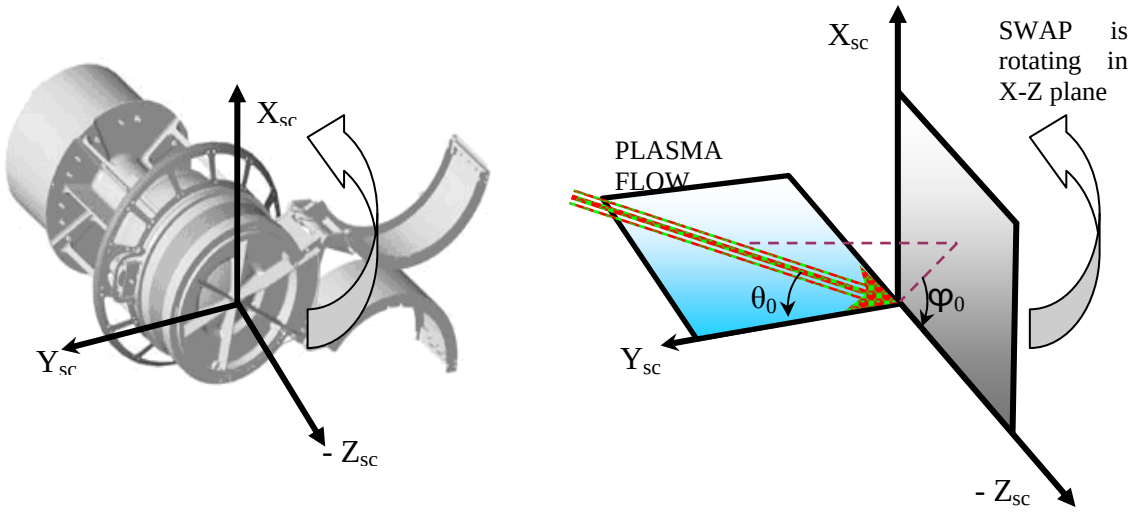

Fig. 2.3: (a) An illustration of the spacecraft coordinate system with respect to the SWAP instrument. The spacecraft rotates along the Ysc axis in the X-Z plane. (b) An illustration of an ion beam entering the instrument in the spacecraft coordinate system.

θ_o ~0^o indicates a purely tailward flow. When the Z_{sc} axis is parallel to Jupiter's spin axis, the instrument measures the flow entering from the east-west (dawn-dusk) direction, i.e., $\varphi_o = 90^o$ and -90^o. An incoming ion beam is observed in the north-south direction, when the Z_{sc} axis of the spacecraft rotates into the dawn-dusk plane, i.e., $\varphi_o = -180^o$, 0^o, and 180^o. Due to the symmetry of SWAP along the center of the aperture, there is an ambiguity of flow direction between spin angles φ_o and $\varphi_o \pm 180^o$. For example, if the ion beam has a substantial velocity component in the cross-tail direction, we cannot determine whether it is an east or west flow component.

An example of a 24-hr energy-time spectrogram is shown in Figure 2.4(a), where the "herringbone" pattern between two red vertical dashed lines is due to the spinning effect. The data coverage of this herringbone pattern is presented in Figure 2.4(b), where the y- and x-axis represent E/q and the spin angle (φ_o), respectively. A corresponding 1-D phase-space density (psd) distribution is presented in Figure 2.4(c), where the red dashed curve is the Gaussian fit.

Without a mass spectrometer, we are not able to verify the observed ion species; hence, H^+ ions have been assumed in our data analysis as a single species. The bulk and thermal velocities are V_0=152.9 and V_{th}=121.1 km s^{-1}, respectively, obtained from the Gaussian fit of Figure 2.4(c). The particle counts of the above example were binned in energy and spin angle as shown in Figure 2.5(a). By using a computational routine, we obtained the maximum counts at spin angles $\varphi_o = 59^o$ and $\varphi_o = -115^o$. We note here that when the herringbone pattern is not present, the plasma can be very hot relative to the bulk energy and/or the flows are nearly tailward ($\theta_o \sim 0^o$) and fall within SWAP's FOV for all spin angles.

In order to complete all energy sweeps of the instrument and to cover all spin angles of the spacecraft in providing a 3-D ion distribution function (except ~13% of 4π sr in the anti-sunward spin direction), the minimum time resolution is approximately one hour. In some case, we need to accumulate few hours of data for a better statistical result especially when the measured count rate is low. Occasionally, it may require 5-6 hours for a complete energy and spin coverage during periods when the spacecraft spin rate changed slightly. The observed ion feature should not vary significantly within the selected time period. We exclude time periods when the majority of data points are below one count level. We also exclude data in our analysis when the instrument only measured the lower or higher tail of the ion distribution. Approximately, only 10% of SWAP data between 500 and 1750 R_J are satisfied for further moment analysis with criterions described above.

In order to obtain fluid moments such as ion density, velocity, and thermal temperature, it is necessary to construct a simulated 3D phase-space density distribution function. A fitting procedure between model results and the data is described in the next section.

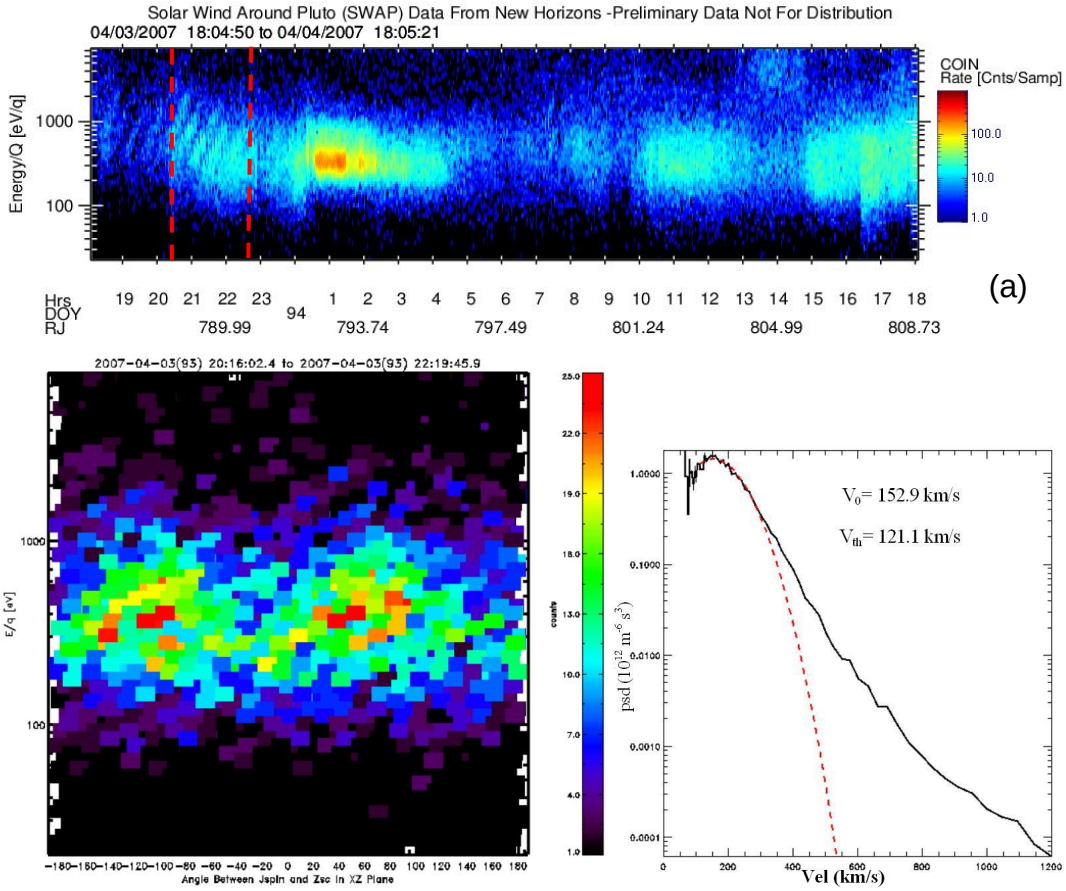

Fig. 2.4: (a) The energy-time spectrogram from 18 UT on Apr. 3 (DOY 93) to 18 UT on Apr. 4 (DOY 94), where an example of the herringbone pattern is highlighted between two red vertical dashed lines. (b) Data coverage of this herringbone pattern in the energy (y-axis) and in the spin angle (x-axis) at 20:16-22:20 UT on Apr. 3. The color represents particle counts. (c) 1-D phase space density (psd) versus velocity corresponding to panel (b), where the red dashed line is the Gaussian fit of the ion distribution.

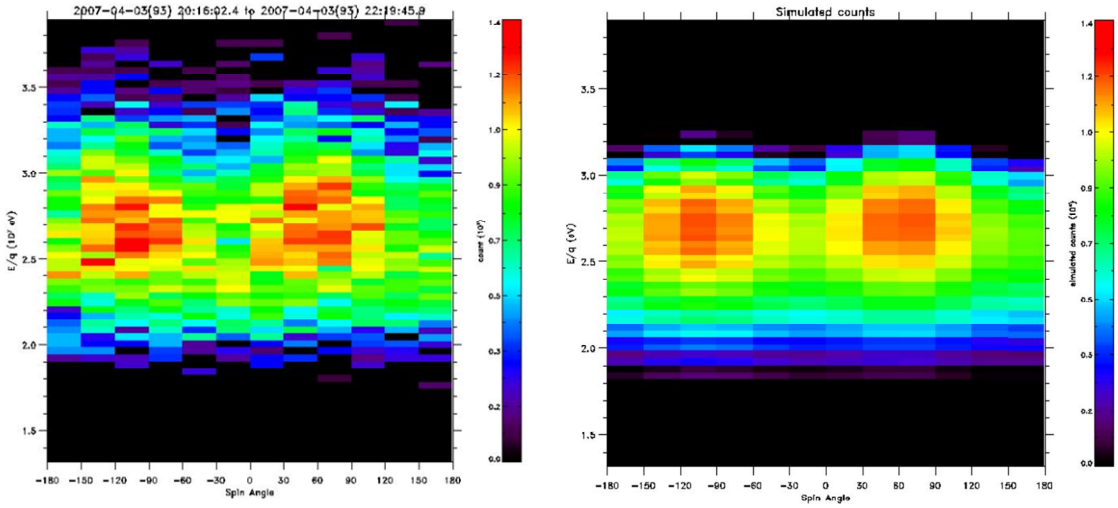

(a) (b)

Fig. 2.5: (a) Binned data of Fig. 2.4(b). (b) Result from the fitting procedure described in Section 2.2.

2.2 Three-Dimensional Phase Space Density Fitting Procedure

The flowchart of a 3-D phase-space density fitting procedure is provided in Figure 2.6. In this code, five input parameters are required: the initial density (N_o), the bulk velocity (V_o), the Mach number (*Mach*), the polar angle (θ_o), and the azimuth angle (φ_o) in the spherical polar coordinate. We refer to Figure 2.3 for the orientation of the ion beam in the spacecraft reference frame. Throughout this paper, the Mach number is defined as the ratio of the bulk velocity to the thermal velocity, $Mach = V_o/v_{th}$. The phase-space density of an isotropic Maxwellian distribution function is

$$f = \frac{N_o}{\pi^{3/2} v_{th}^3} exp\left[- \frac{(v_x - V_{ox})^2 + (v_y - V_{oy})^2 + (v_z - V_{oz})^2}{v_{th}^2} \right],$$

where the thermal speed and three velocity components are

$$v_{th} = \sqrt{2k_B T_{th} / m_i} \ ,$$

$$V_{ox} = V_o \ sin\theta_o \ sin\varphi_o \ ,$$

$$V_{oy} = V_o \ cos\theta_o \ , \quad \text{and}$$

$$V_{oz} = V_o \ sin\theta_o \ cos\varphi_o \ .$$

Again, the *y* axis is the spacecraft spin axis. Throughout this paper, the "tailward" component represents the velocity component along the y-axis (i.e., along the spacecraft trajectory), while the "non-tailward" component is in the x-z plane perpendicular to the spin axis.

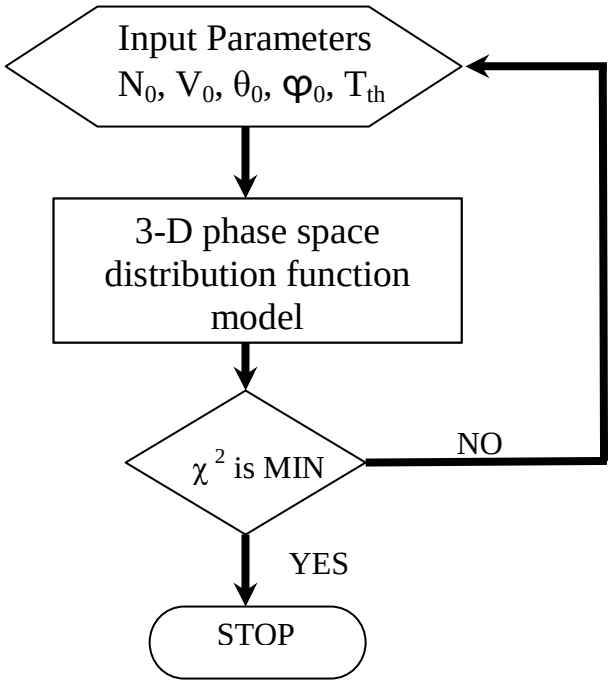

Fig. 2.6: A flowchart of the 3-D phase-space density fitting procedure.

We are able to validate our model by integrating the phase-space densities in 3-D to obtain the density, velocity, and thermal temperature as

$$N_0 = \int f d^3v \,,$$

$$\vec{V}_0 = \int \vec{v} f d^3v / N_o \,,$$

$$T_{th} = m_i \int (\vec{v} - \vec{V}_o)(\vec{v} - \vec{V}_o) f d^3v / (3k_B N_o) \,.$$

Results from the integration are nearly identical to the input values within numerical errors. The integration is replaced by a summation in the numerical calculation.

Since the instrument measures the count rate, we convert the phase space density into charged particle counts with calibration parameters provided by the SWAP instrument team [*McComas et al.,* 2008] such that

$$C_{Model} = \Delta t A_{eff} \Delta\alpha \frac{\Delta E}{2E} v^4 \sum_{-138^o}^{138^o} \Phi f \,,$$

where Δt = 0.39 *sec* is time resolution, A_{eff} = 3.3×10^{-2} *cm*^{2} is effective area, $\Delta\alpha$ = 10^o is the smaller FOV, and $\sum_{-138^o}^{138^o} \Phi$ = 276^o is the larger FOV, $\Delta E/E$ =0.085 FWHM is energy resolution of the electrostatic analyzer (ESA), and *v* is the velocity which is converted from the energy by $v = \sqrt{2E/m_i}$.

Finally, we will compare our model result with the data to obtain the moments with the best Chi-Square fitting [*Press et al.,* 1989]. The maximum likelihood estimate of the model parameters is obtained by minimizing the "chi-square" quantity

$$\chi^2 = \sum_{i=1}^{N} \frac{\left(C^i_{Measure} - C_{Model}\right)^2}{\sigma^2} \,,$$

where $C^i_{Measure}$ and C_{Model} are measurement counts and simulated model counts. Here, we assume the error is equal to the square root of the measured counts, $\sigma = \sqrt{C^i_{Measure}}$. *N* represents the number of measurement points with counts are higher than the one-count level.

A very good fit is defined as $\chi^2 \leq N - M$, where *M* is the number of input parameters (*M*=*5*). The fitting procedure is iterated until the simulated result achieves the minimum chi-square value.

SWAP measures ions in E/q; hence, it is not designed to distinguish various ion species. Ions with an atomic mass of one and a positive charge of one, i.e., protons, are assumed in the fitting procedure in our initial study. This assumption does not imply that protons are the dominatnt species in Jupiter's magnetotail; rather, the results of *McComas et al*. [2007] suggest that the tail plasma is a variable mixture of heavy and light ions. *McComas et al*. [2007] indicated that the ratio of counts detected in SWAP's secondary and primary detectors provides an approximate measure of ion mass (see their Figure 3b). The instrument response to various ion species is currently conducted in a separated study at SwRI, which is not covered in this thesis. The moments obtained from our fitting procedure can be scaled up (for density) or down (for velocity) based on the square root of the mass per charge (m/q) ratio for heavier ion species when the result of the instrument response is available.

The fitting result of the distribution shown in Figure 2.5(a) is presented in Figure 2.5(b) as an example. The most probable estimated density, velocity, thermal temperature, and Mach number for protons are ~ 8.5×10^{-3} cm^{-3}, 157 $km\ s^{-1}$, 163 *eV*, and 0.89, respectively. The ion beam entered the detector with θ_o ~ 47^o, corresponding to a tailward velocity component of 107 $km\ s^{-1}$ and a non-tailward component of 115 $km\ s^{-1}$ at spin angle φ_o ~61^o or -109^o. We should note here that an isotropic Maxwellian distributions is prescribed at each of the two maximum likelihoods of spin angles, hence, we obtain two values for each fluid moment due to the ambiguity in the non-tailward flow direction (see Section 2.1). The best-fit parameters are the averages of these two maximum likelihoods except for φ_o. For the case presented in Figures 2.5(a) and 2.5(b), the minimum value of $\chi^2/(N-M)$ is 0.89, where *N* = 547.

CHAPTER 3

RESULTS

After careful examination of the fitting procedure, we were able to obtain the characteristics of charged particles between March 23 and May 12, 2007 (i.e, ~500-1750 R_J). We treated all measured ions as a single species, H^+. It should be noted that multiple species could be present simultaneously; however, we are not able to distinguish them apart because the instrument was designed to collect all ions without a mass spectrometer. Our model is able to fit data for two ion species with distinct energy peaks in the spectrogram. In general, the plasmas in the solar wind have higher densities and lower thermal velocities compared to those in the magnetosphere.

3.1 Moments' Variation Over a 24-hr Period

The fitting procedure and input parameters have been described in Chapter 2 to obtain ion fluid moments. In this section, we describe variations of ion moments over 24 hours of the spacecraft's journey, i.e., 2.5 Jupiter days (10 hr per Jupiter rotation). It should be noted that results vary as the spacecraft traveled through different portions of the distant tail. Here, we select to present two segments of SWAP data and demonstrate various characteristics of ions (Case A) between 620 and 640 R_J and (Case B) between 1179R_J to 1193R_J.

3.1.1. Case A

Ion moments are displayed in Figure 3.1 and Figure 3.2 from 619 to 640 R_J, i.e., 08UT on 03/27/2007 (DOY 86) to 08UT of 03/28/2007 (DOY 87), where the energy spectrogram, density, velocity, number flux, Mach number, temperature, thermal pressure, polar angle (θ_o), flow components, spin angle (φ_o), and velocity vector are plotted in Panels (a)-(k), respectively.

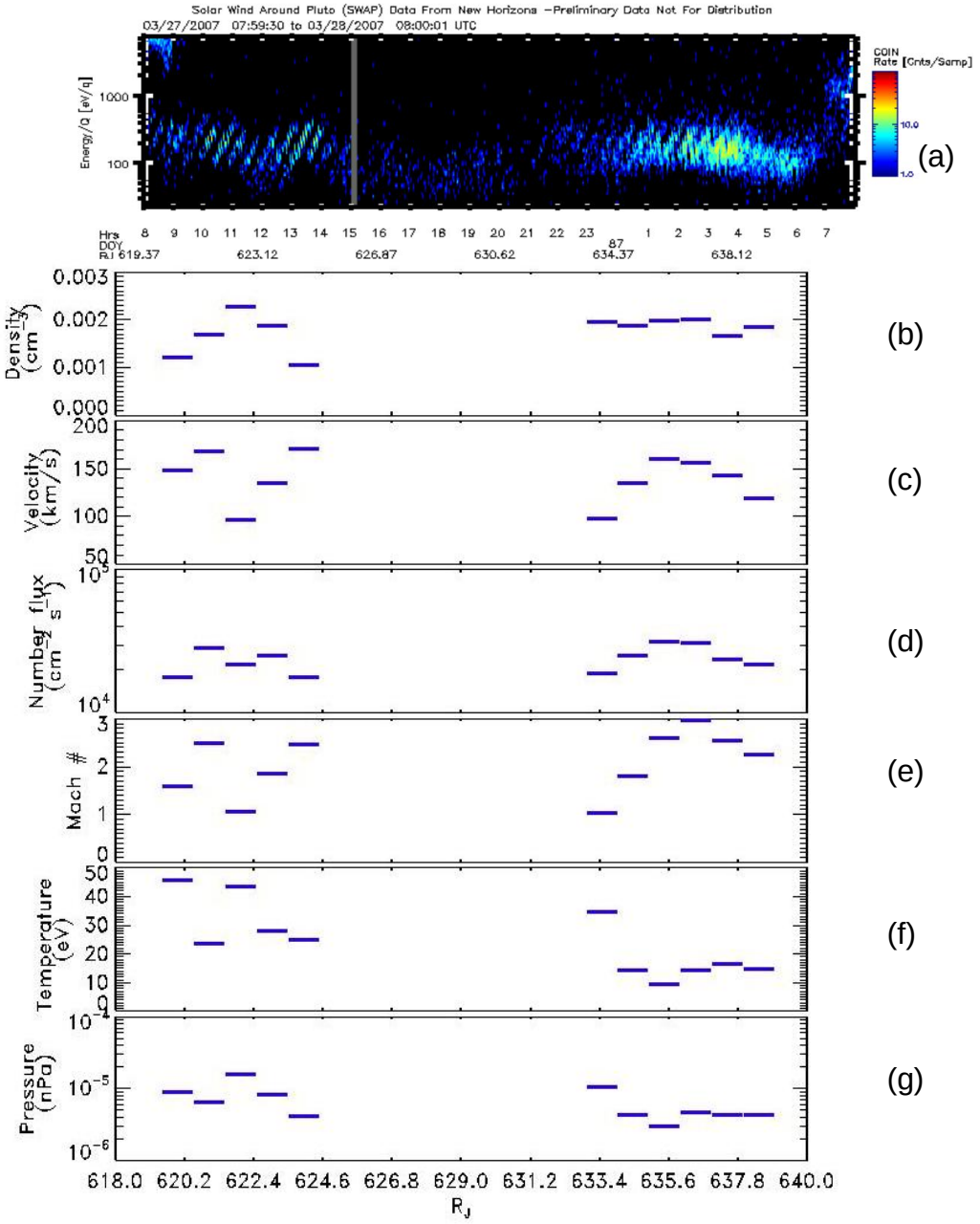

Fig. 3.1: (a) A 24-hr energy spectrogram from 08UT on Mar 27, 2007 to 08 UT on May 28, 2007. (b) The density, (c) velocity, (d) number flux, (e) Mach number, (f) temperature, set (g) pressure. Fig 3.2 shows the next set of moments for the same event

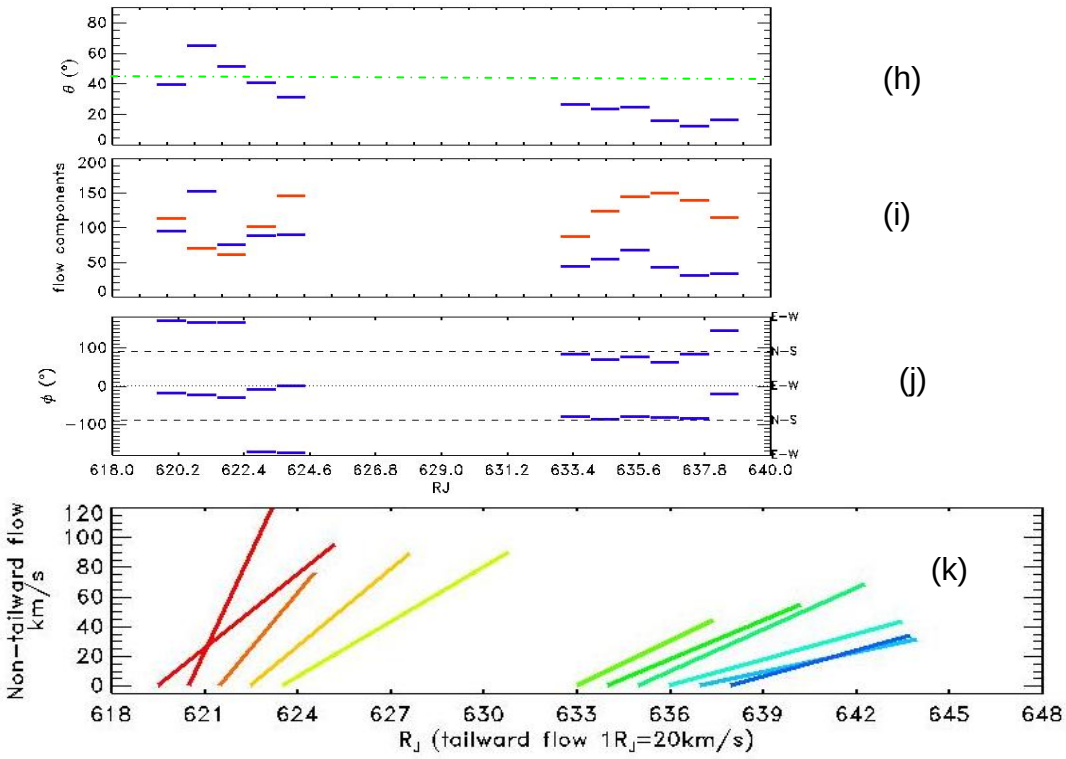

Fig. 3.2: For the event in Fig 3.1- (h) polar angle, (i) flow components, and (j) spin angle from 618 to 640 R_J. Red and blue bars in panel (i) represent the tailward and anti-tailward flow components, respectively. (k) The 2-D velocity vectors between 618 and 648 R_J, where 1 R_J represents 20 km s-1 in the x-axis.

Though the moments are split into two figures the panels are labeled continuously from (a) to (k) across two figures. It should be noted that the length of the x-axis is slightly different in panels (a) and (k) compared to other panels. The distance from Jupiter center is labeled under the x-axis in panels (a), (g), (i), and (j), while the universal time is only labeled under panel (a). The resolution of each data point in panels (b)-(j) is approximately one hour, corresponding to each horizontal bar. The red and blue horizontal bars in panel (i) represent the tailward ($V_Y=V\cos\theta_0$) and non-tailward flow ($V_{XZ}=V\sin\theta_0$) components. The bottom panel of Figure 3.2 provides a visual presentation of the 2-D velocity vectors, where 1 R_J represents 20 km s^{-1} in the x-axis.

Based on the energy spectrogram in panel (a), energies of observed ions are similar within a range of 10s-100s eV; however, the count rate varies, where the highest count rate observed between 01 and 06 UT on DOY 87 and the lowest from 15 to 23 UT on DOY 86. The region with the lowest count rate is excluded in our data analysis because particle counts are near the noise level of the instrument.

In panel (b), the density between 08 and 14 UT on DOY 87 shows a hump like distribution with a local maximum of 2.26×10^{-3} cm^{-3} at ~622.43R_J, while the local minimum of velocity is ~95 km s^{-1} in panel (c). The density between 23UT on DOY 87 to 05UT on DOY 88 is nearly uniform. Many ionospheric physicists use the number flux as a physical index for the ionospheric outflow. The number flux is in the same order, $2\text{-}3 \times 10^4$ cm^{-2} s^{-1}, in panel (d). The Mach number (V_o/V_{th}) ranges between 1 and 3 during this period, which is much lower than that in the solar wind (≥6). The Mach number calculated here is another representation of the temperature calculated here. But a quick look on this number gives an idea of presence of solar wind particles. The ion temperature (panel f) and pressure (panel g) have a clear anti-correlation with the Mach number (panel e). We note that ion pressures calculated here are based on particle counts measured within the SWAP energy range. The higher energy particles observed by another plasma instrument PEPSSI onboard New Horizons should account for the majority of the total thermal pressure. However in an attempt to calculate the magnetic field in zeroth order discussed in the last chapter, we assumed contributions from both lower and higher energies to be of same order. Based on the pressure balance theory [Sittler et al.,1987], the combination of these two particle pressures from two instruments along with the magnetic field pressure in the magnetosphere account to balance the solar wind pressure.

In general, the gaps within the herringbone pattern (panel a) increase with increasing polar angle (panel h); hence, gap for θ_o ($\leq 30^o$) in the second block of data (633-638 R_J) in panel (h) is lower than those ($\theta_o \geq 30^o$) in the first block (619-625 R_J). When $\theta_o \geq 45^o$, the non-tailward

component is greater than the tailward component. It should be note that a pure tailward flow (θ_o=0^o) does not associate with herringbone patterns. The non-tailward component (Vxz) exists when $\theta_o > 0^o$, and the information of the spin angle φ_o is present in panel (j). During this period, the first block of plasma flows is dominated in the east-west direction, while the second block of flows are primarily in the north-south direction.

3.1.2. Case B

Ion moments from 1179 to 1193 R_J are displayed in Figure 3.3 and Figure 3.4, i.e., 06:40UT to 22:20 UT on 04/21/2007 (DOY 111). The count rate immediately before and after the plotting period is too low to be included in our analysis. The format of Figure 3.3 and Figure 3.4 is the same as that of Figure 3.1 and Figure 3.2, except that in panel (k) 1 km s^{-1} is represented by 1 R_J in the x-axis.

During this period, the velocity flow shown in panel (c) is nearly constant with an average velocity of 128 km s^{-1}. Temperatures of 2-5 eV shown in panel (f) are the lowest within the entire range of 500-1750 R_J. Variations in number flux (panel d) and pressure (panel g) reflect the variation in density (panel b). The polar angles (panel h) are less than 20^o throughout this period indicating a strong tailward flow component (panels i and k). The non-tailward velocity component is small (< 40 km s^{-1}) and it slowly transitions from the north-south direction to the east-west direction from 1179 to 1193 R_J.

Overall, the variation in plasma characteristics of Case B is the smallest of the entire magnetotail dataset between 500 and 1750 R_J.

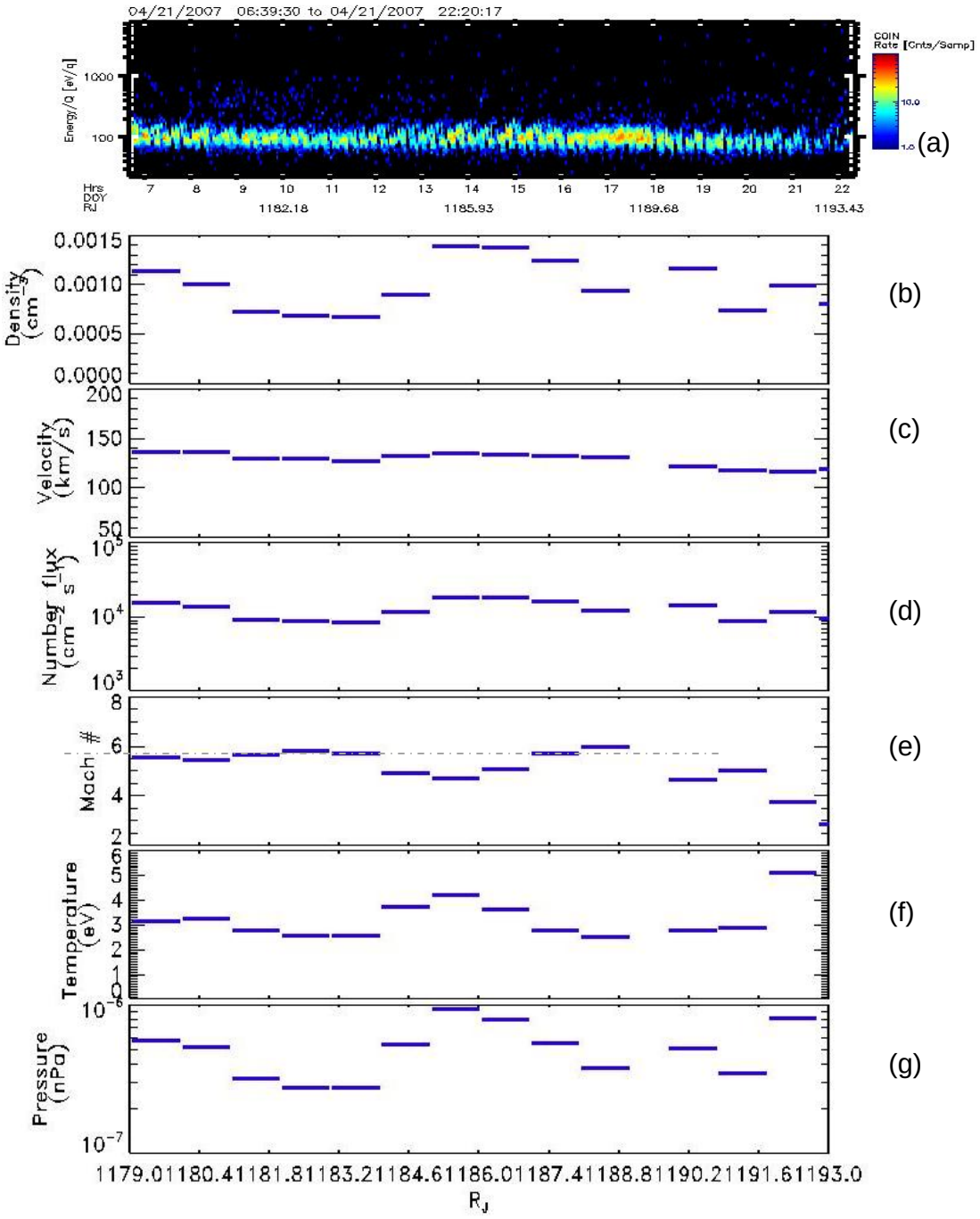

Fig. 3.3: (a) A 16-hr energy spectrogram from 06:39UT to 22:20 UT on Apr 21, 2007. (b) The density, (c) velocity, (d) number flux, (e) Mach number, (f) temperature, (g) pressure. Fig 3.4 shows the next set of moments for the same event

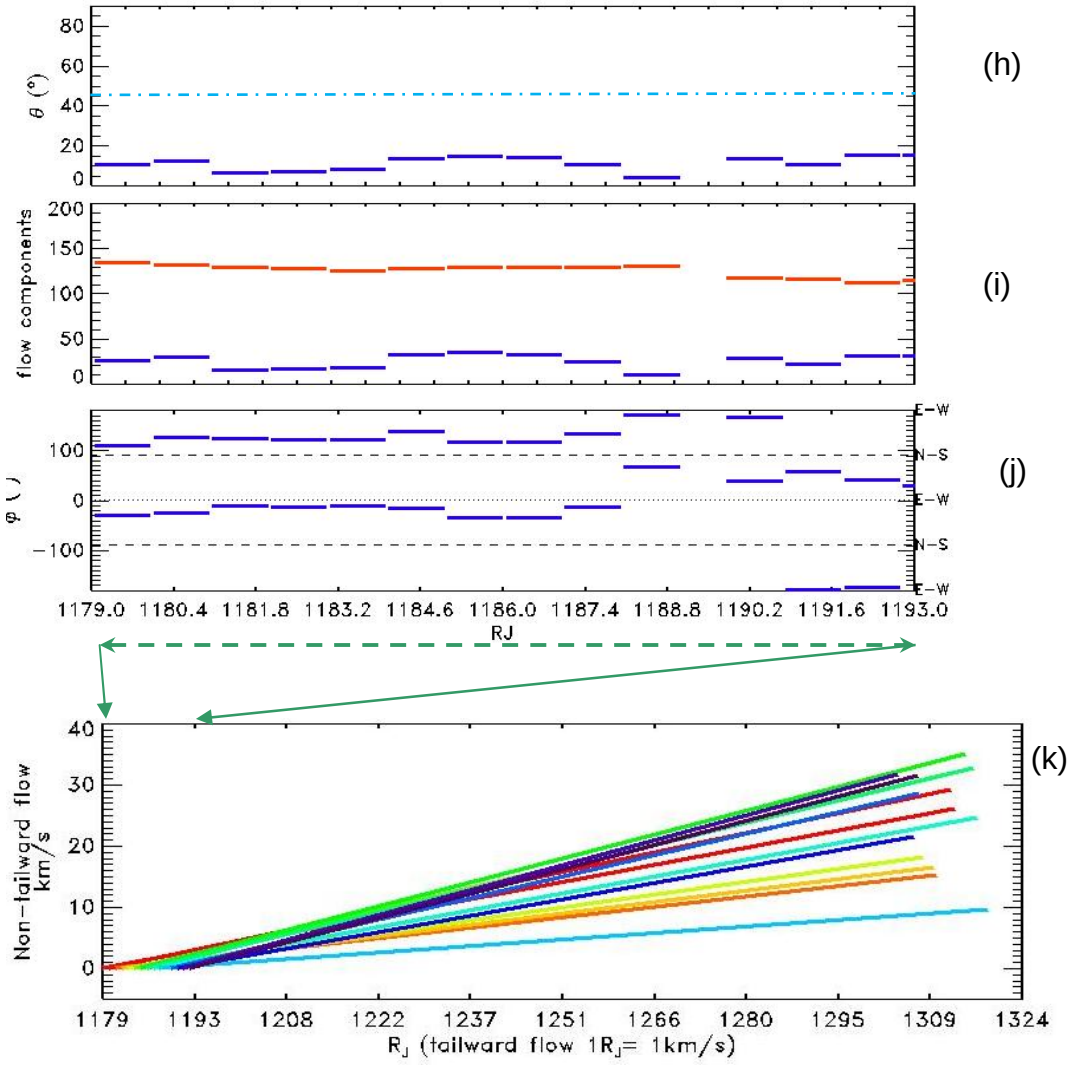

Fig. 3.4: For the event in Fig 3.3- (h) polar angle, (i) flow components, and (j) spin angle from 1179 to 1193 R_J. Red and blue bars in panel (i) represent the tailward and anti-tailward flow components, respectively and (k) the 2-D velocity vectors between 1179 and 1324 R_J, where 1 R_J represents 1 km s-1 in the x-axis.

3.2 Variations Over 500-800 R_J

We remind readers that the NH spacecraft started spinning at ~500 R_J on March 23 (DOY82) and entered the solar wind on May 12 (DOY 132), 2007. The 3rd and 4th energy spectra shown in Figure 2.1 are displayed in Figure 3.5 again. The red dashed curves between 600-1000 R_J in Figure 3.5 indicate regions where a 3-4 day quasi-periodicity may exist reported by McComas et al. [2007]. Ion moments from 537 to 800 R_J are displayed in Figure 3.6 and Figure 3.7, where the format is the same as that of Figure 3.3 and Figure 3.4. Data presented in Figure 3.1 and 3.2 (Case A) are included in Figure 3.6 and 3.7 between two vertical dashed lines. 15% of the data within this period (DOYs 82-94) met our criterion for moment analysis described in Chapter 2. We note here that, between DOY 95 and 104, we were only able to process 12 hours of data to obtain 5 average points for each fluid moment (i.e., 5%, not shown here). We are not able to verify the quasi-periodicity described by McComas et al. [2007] from fluid moments due to insufficient information.

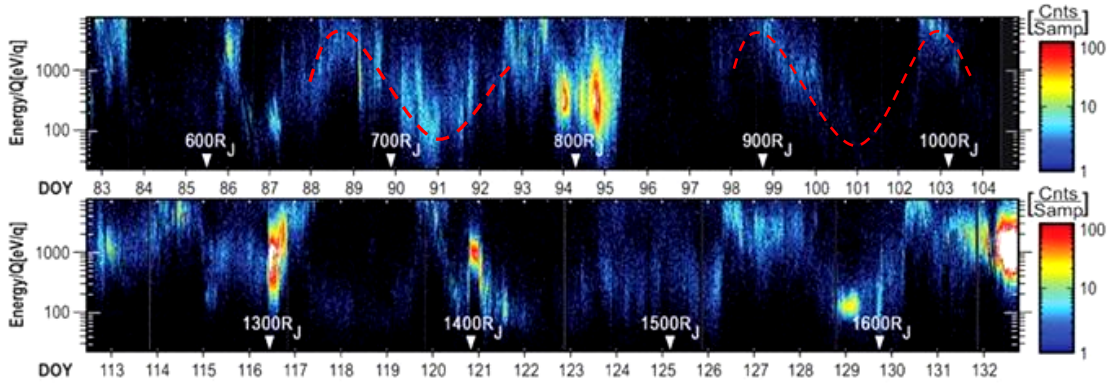

Fig 3.5: Energy spectrogram from ~500-1750R_J. Red dashed curves mark the 3-4 days variation as mentioned in McComas et al, 2007. Also from DOY 83 NH started spinning. (after McComas et al, 2007)

It is interesting to point out that the polar angles θ_o (panel h) resemble a sinusoidal shape as that shown in the energy spectrogram (panel a). This period presents the diversity of flow directions (see panels i-j), as well as fluid moments. A summary of the minimum and maximum of fluid moments is listed in Table 3.1.

The region between 670 and 770 R_J is an ideal period to verify the density (panel b) and velocity (panel c) from our fitting procedure in comparison with the energy spectrogram (panel a). The bulk velocity decreases with decreasing energy. Low energy ions dominate the phase-space density resulting in higher densities.

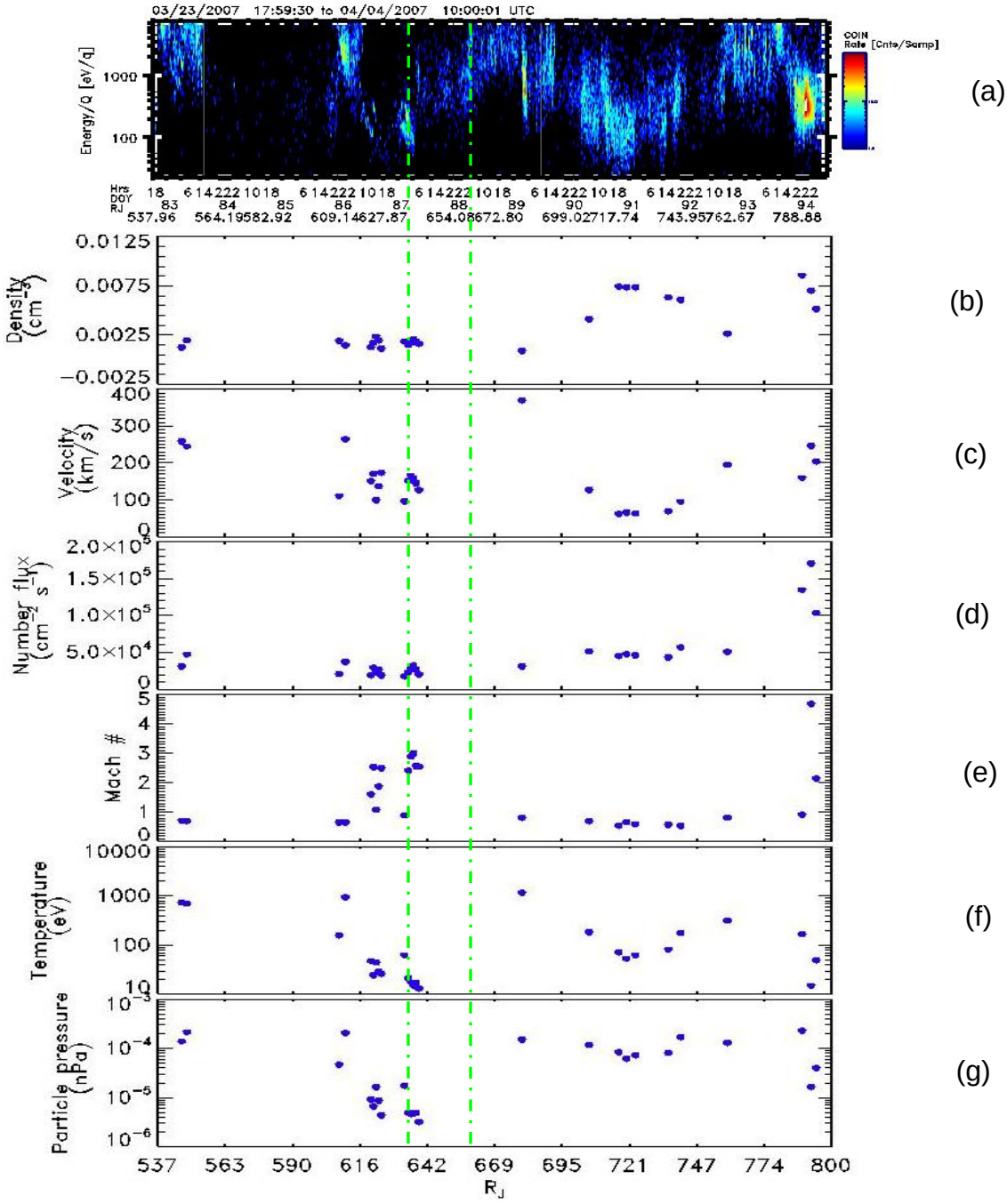

Fig 3.6: (a) Energy spectrogram from 537-800R_J. (b) The density, (c) velocity, (d) number flux, (e) Mach number, (f) temperature, (g) pressure. Fig. 3.7 shows the next set of moments for the same event

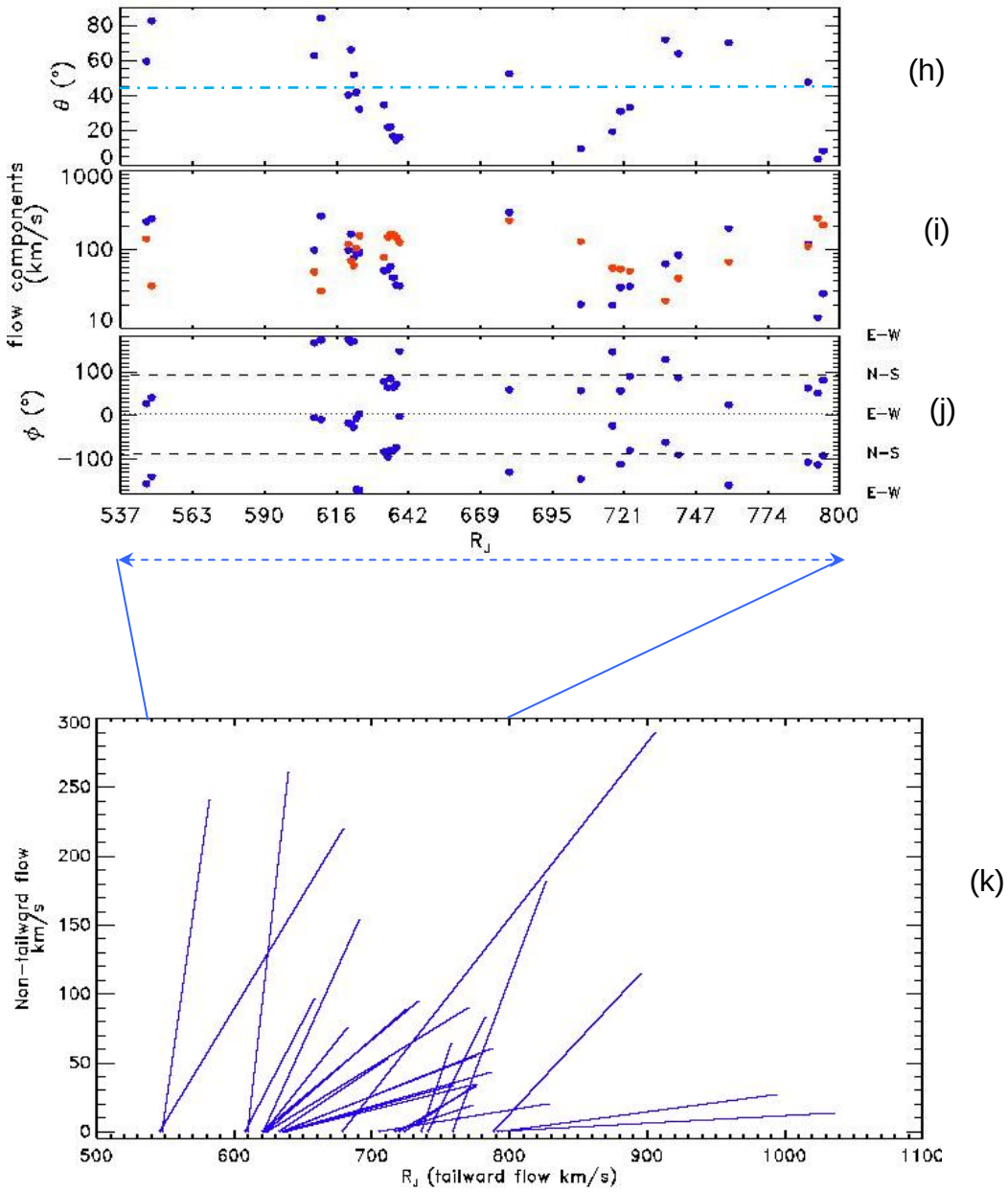

Fig 3.7: For the event in Fig 3.6- (h) polar angle, (i) flow components, and (j) spin angle from 537 to 800 R_J. Red and blue bars in panel (i) represent the tailward and cross-tail flow components, respectively. (k) The 2-D velocity vectors between 537 and 800 R_J, where 1 R_J represents 1km s-1 in the x-axis.

Table 3.1: A summary of ion moments in the Jovian magnetotail from in 500-800R_J

	Min	Max
Density (cm^{-3})	0.000551	0.00868
Velocity (km s^{-1})	60.13	367.56
Mach#	0.51	4.64
Temperature (eV)	0.62	1116.87

3.3 The Solar Wind Entry

After a 2.5-month journey in Jupiter's system, the NH spacecraft entered the solar wind on May 12 (DOY 132), 2007. NH continuously crossed the boundary between the magnetosphere and the solar wind from 1750 to 2500 R_J (see the 5th spectrogram in Figure 2.1) until instruments were switched into the hibernation mode.

An example of ion characteristics in the boundary layer and the solar wind is shown in Figure 3.8 from 15:30 UT on May 11 to 17:30 UT on May 12. A transition between the magnetosphere and the solar wind can be identified at ~06:30UT marked as the vertical line in the spectrogram (panel a). The density (panel b) increases two orders of magnitude from 0.001 cm^{-3} at 1650 R_J, 0.01 cm^{-3} at ~1652 R_J, to ~ 0.1 cm^{-3} at > 1655 R_J, while the velocity (panel c) remains in the same order with an averaged value of 445 km s^{-1}. The Mach number (panel d) increases with decreasing temperature (panel f). The Mach number increases from an averaged value of ~2.5 to 6 across the boundary (marked by the vertical line). Based on the characteristics of fluid moments, SWAP measured solar wind particles at distance greater than 1652 R_J. The solar wind primarily flows in the anti-sunward direction (panel i) with a minor north-south component (panel j). Table 3.2 summarizes the average values of ion characteristics across the boundary between the magnetotail and the solar wind.

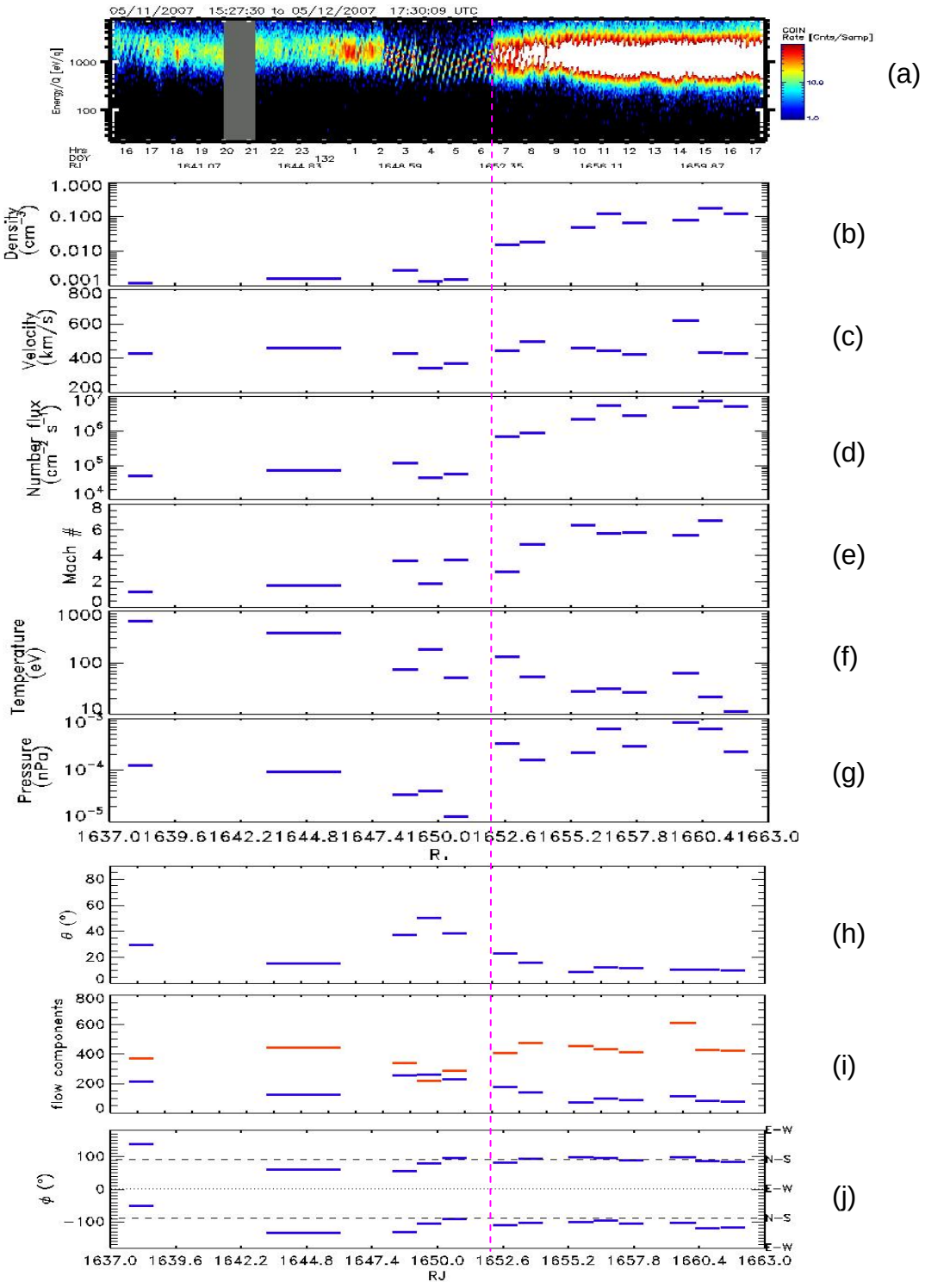

Fig 3.8: Moments shown in different panels from 1637 to 1663R_J. At ~ 1652 R_J, NH enters the solar wind.

Table 3.2: Change in average values of the moments as NH enters the solar wind from the magnetotail on DOY 132

	Magnetotail	Solar wind
Density (cm^{-3})	1.7×10^{-3}	0.817×10^{-1}
Velocity ($km\ s^{-1}$)	405.66	469.61
Mach#	2.4	5.86
Temperature (eV)	268.21	46.44
Pressure (nPa)	$6.08\ 10^{-5}$	1.66×10^{-3}

3.4 Two Species Analysis

The SWAP instrument occasionally measured ions with two distinct peaks in the energy spectrogram indicating the presence of additional ion species. Three examples are presented in Figure 3.9 where panels a-c show two-species observations in the magnetotail at 1230-1500UT on Apr. 27, the boundary layer at 0130-0330UT on May 19, and the solar wind between 1812 UT on Jun. 8 and 1700UT on Jun. 9, respectively. Based on the ratio between the secondary and primary counts of the SAWP instrument, McComas et al. [2007] suggested that the low-energy species at 1230-1500UT (in panel a) is H^+, while the species with higher energies are H_3^+ ions. With the proper input of ion mass, the result of fluid moment analysis supports their conclusion that both ion species share the same convection velocity (result not shown here).

Initial analysis of two ion species from 2229-0033 UT (marked between two vertical lines in Figure 3.9c) is shown in Figure 3.10, where the left panel presents the binned ion counts in E/q versus the spin angle and the right panel shows the 1-D phase-space density versus

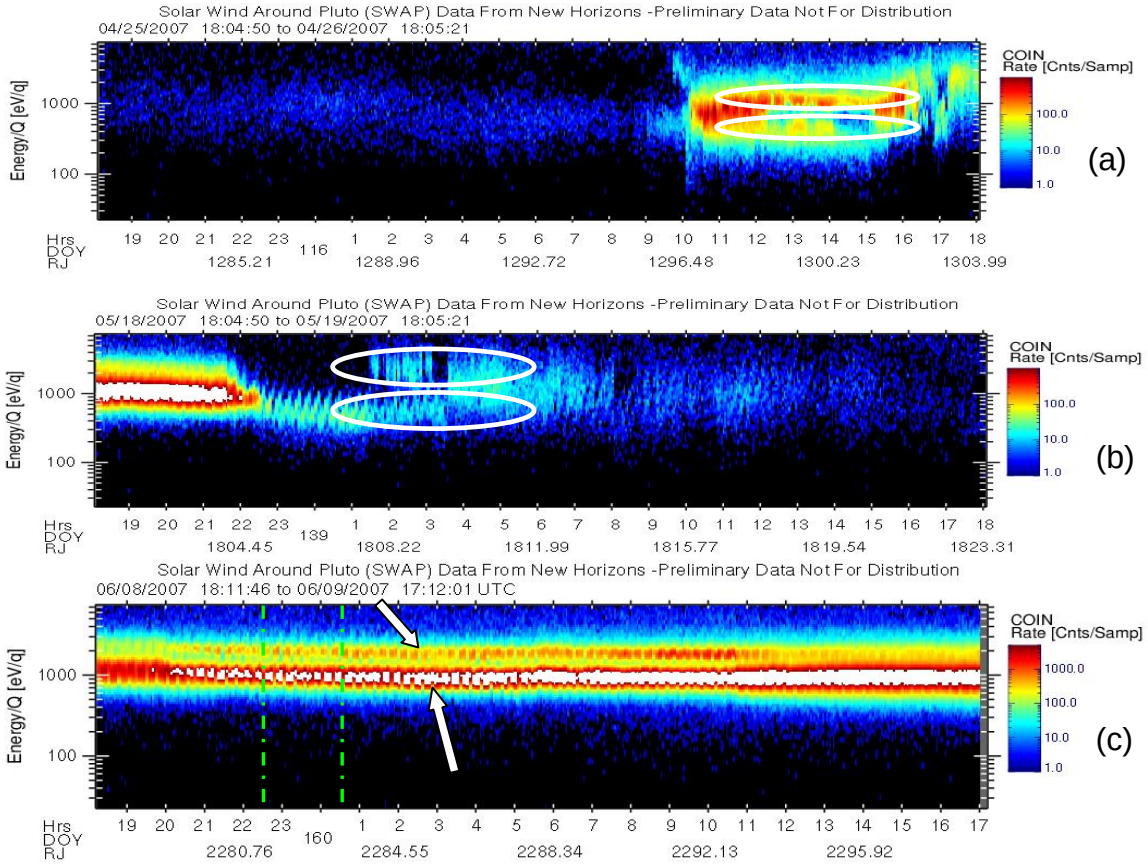

Fig. 3.9: Energy spectrogram from SWAP showing the presence of two separate energy bands at different places in the magnetotail. Since SWAP measures E/q, this clearly implies presence of multiple species with at least two different E/q values.

velocity. One species peaks at 460 km s^{-1} (~1000 eV/q) and the other at 633 km s^{-1} (~ 2000 eV/q). If both species share the same convection speed, the mass-per-charge ratio is 1:2, which is consistent with the solar wind composition: $^{1}H^{+}$ is the dominant species and $^{4}He^{++}$ (α particle) is the secondary.

McComas et al. [2007] reported that the ratio of counts detected in SWAP's secondary and primary foils provides an estimation of ion mass. Ground foil calibration for a heavy ion (1 *keV* N^{+}) produced a ratio of 2.7, while a light ion (1 *keV* H^{+}) had a ratio of ~ 1.3. A detailed laboratory test has been conducted at SwRI. Although we are not able to quantitatively

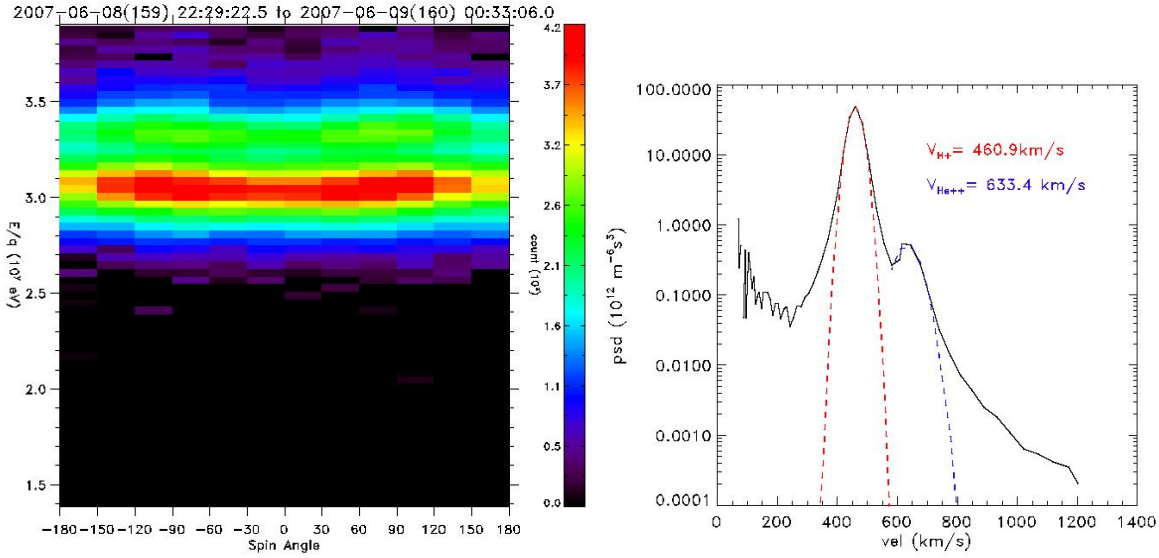

Fig 3.10: (left) Energy coverage for 06/08/2007 from 22:29:22 -00:33:06 UT. Two clear energy peaks shows presence of at least two species. (right) 1-D psd v.s. velocity, where red and blue dotted lines in the right panel are the Gaussian fitting for the higher and lower energy

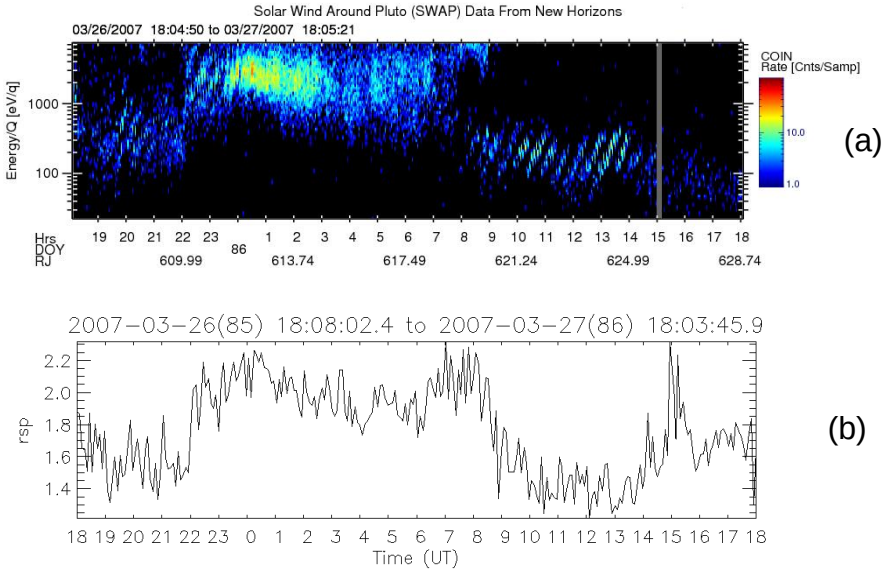

Fig 3.11: An example showing secondary to primary count ratio from SWAP can be used to determine the heavier species from the lighter one. Panel (a) shows the spectrogram from 18UT of DOY 86 to 18UT of DOY 87. Panel (b) displays the secondary to primary counts during this period.

determine the mass, we can estimate the source of ions based on the ratio of secondary to primary counts. An example is shown in Figure 3.11. The higher energy portion of the spectrogram (between 22 and 08 UT in the top panel) consists with heavier ions where the origin of ions may come from Io, while the lower energy ions (before 22 UT on Mar 26 and after 8 UT on Mar 27) may originate from Jupiter's topside ionosphere or the solar wind where H^+ ions are the primary species.

3.5 Summary of Fluid Moments from 500 to 1750 R_J

In this section, we summarized ion moments for the entire magnetotail fly-by from 500 to 1750 R_J in Figure 3.12. The corresponding energy spectrogram is shown in Figure 3.5. The densities of the magnetotail are generally less than 0.01 cm^{-3}. We might not be able to obtain densities lower than 10^{-3} cm^{-3}, because count rates were near or below the instrument noise level. As discussed in the previous section, the NH spacecraft enters the solar wind at ~1650 R_J, where the density is on the order of 0.1 cm^{-3}. The diversity of flow directions is noticeable between 500-1000 R_J, while a strong tailward flow with a few exceptions is shown after 1130 R_J. Temperatures in the magnetotail vary from < 10 to ~1000 eV, while low-energy ion pressures change between 10^{-7} and 10^{-4} nPa. Our results confirm that Jupiter has a highly structured long magnetotail with a diversity of plasma populations. The minimum, maximum, and average values of ion moments in Jupiter's magnetotail (exclude the solar wind) from 500–1500 R_J are summarized in Table 3.3.

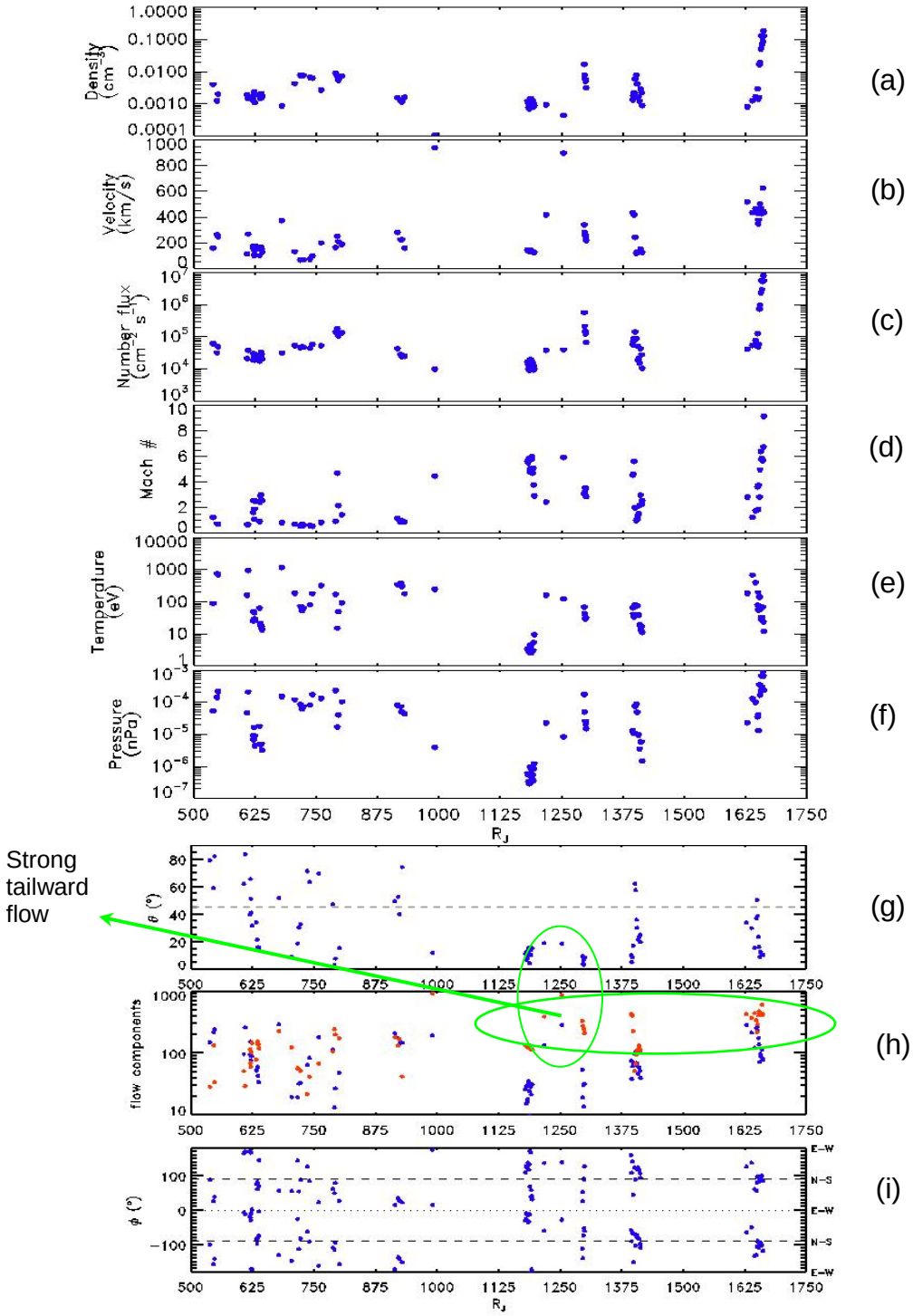

Fig 3.12: (a) The density, (b) velocity, (c) number flux, (d) Mach number, (e) temperature, (f) pressure, (g) polar angle, (h) flow components, and (i) spin angle from from 500-1750R_J. Red and blue dots in panel (i) represent the tailward and non-tailward flow components.

Table 3.3: Summary of ion moments in the Jovian magnetotail from 500-1500R_J

	Min	Max	Avg
Density (cm^{-3})	1 X 10^{-4}	1.6 X 10^{-2}	2.8 X 10^{-3}
at (R_J)	990.44	1295.72	
Velocity (km s^{-1})	60.13	936.49	198.52
at (R_J)	716.58	990.44	
Mach #	0.51	5.94	2.66
at (R_J)	740.75	1188.52	
Temperature (eV)	2.52	1116.87	114.47
at (R_J)	1188.52	678.88	

CHAPTER 4

DISCUSSIONS AND CONCLUSIONS

This thesis is the first publication of ion moments obtained from the SWAP instrument onboard NH with detailed descriptions of data selection criteria and 3-D Maxwellian fitting procedures. By taking an advantage of the particle instrument designed for Pluto, the spinning of the NH spacecraft provided us a chance to obtain almost 3-D ion distributions along a path through Jupiter's enormous magnetotail. The best resolution of each complete distribution of SWAP is an approximately an hour, which is considered to be inadequate for modern earth-orbiting satellites. In some cases, we needed to accumulate 2 or 3 hours of data in order to process our statistic fitting routine. A slight change in spin rate could reduce the resolution to 5-6 hours such as the data obtained on April 4, 2007. Unfortunately, almost 90% of fly-by data do not meet our criteria due to either low count rates, rapid changes in particle characteristics, or incomplete distributions limited by the instrument's energy coverage. Despise many limitations, NH successfully fulfills its Jupiter's fly-by mission and provides the science community with data filling the gap between Jupiter's middle magnetosphere (Galileo) and the distant tail (Voyage 2 fly-by).

As summarized in Section 3.5 and Figure 3.9, Jupiter's magnetotail is very dynamics with a diversity of ion properties. The ion density in the magnetotail varies by 2 orders of magnitudes between 10^{-4} and 1.6×10^{-2} cm^{-3}. Due to NH's unique trajectory, we are unable to compare our results directly with other satellites. The highest density 1.6×10^{-2} cm^{-3} observed at 1295 R_J by NH is lower than 0.05-0.1 cm^{-3} observed at distance >50 R_J from Galileo [reviewed by Khuruna et al., 2004]. The majority of magnetotail densities fall in the same order, 10^{-3} cm^{-3},

as those observed by Voyager 2 at ~6000-8000 R_J [see Table 2 of Kurth et al., 1982]. The lowest density estimated from our fitting procedure is 10^{-4} cm^{-3} at ~ 1000 R_J.

Although our instrument is not able to detect the sunward flow due to its geometry, we observed flows of 50-400 km s^{-1} nearly in every direction between 0^o and 90^o, particularly at distances less than 1000 R_J. The tailward flow dominates at distances greater than 1130 R_J. An anti-sunward flow of ~200 km s^{-1} at 100 R_J observed by Galileo supporting the magnetospheric "wind" scenario reported by Voyager [Khuruna et al., 2004]. Our results from NH suggested that the magnetotail beyond 500 R_J is very complex and turbulent.

Lewis [1997] reported that the solar wind density and velocity is ~0.5 cm^{-3} and 500 km s^{-1} at 5.2 AU. Based on the gas dynamics theory [Spreiter and Stahara, 1985], the solar wind pressure at the distant flank is estimated to be ~0.04 nPa. The total pressure consists of the kinetic and thermal pressures of particles as well as the magnetic pressure. Because the interplanetary magnetic field is very weak and the thermal velocity is much lower than the solar wind speed, both magnetic and thermal pressures can be neglected. With a density of 0.1 cm^{-3} and a speed of 470 km s^{-1} observed from NH at 1650 R_J, the solar wind pressure is estimated to be ~0.02 nPa, which is comparable with the result estimated from the gas dynamic theory.

The low-energy ion thermal pressures obtained from SWAP in Jupiter's magnetotail vary by three orders of magnitudes ranged from $2.7x10^{-7}$ to $2.2x10^{-4}$ nPa, which are too small to account for the solar wind pressure balance. In an attempt to make zero order estimate of the magnetic field at ~1650R_J, we tried to balance the pressures from solar wind and magnetotail. Since the ram pressure acts parallel to the tail, only the thermal pressure (nkT) of the particles in solar wind takes part in the pressure balance. Assuming only protons in the solar wind and using density of 0.1 cm^{-3} at ~1650 R_J derived from SWAP data we get $P_{sw\text{-}thermal}$ ~ 7.36 X 10^{-4} nPa. For the magnetotail, if we assume that the higher energetic particles (beyond SWAP's range) which are detected by onboard PEPSSI instrument also contribute an equal amount of

thermal pressure as by the low energy ions, i.e., 6.08 X 10^{-5} nPa (from Table 3.2), we can write the pressure balance equation as:

$P_{sw} = P_{total} = P_{lowenergy} + P_{highenergy} + P_{B\text{-}magnetotail}$

$P_{sw} = 2*6.08*10^{-5} + B_0^2/2\mu_0$

⇨ $7.36 \text{ X } 10^{-4} = 12.16*10^{-5} + B_0^2/(2*4*3.14*10^{-7})$

⇨ $B_0 = 1.24 \text{ X } 10^{-9} \text{ T} = 1.24 \text{ nT}$

[here P_{sw}= solar wind total pressure, $P_{sw\text{-}thermal}$ is solar wind thermal pressure, $P_{lowenergy}$ and $P_{highenergy}$ are thermal pressures contributed from low (from SWAP) and high (from PEPSSI) energy particles and PB-magnetotail is the magnetic pressure in the magnetotail]

To compare with other literatures we convert this in cgs units which give a magnetic pressure: $B_0^2/2\mu_0 \sim 6.1 \text{ X } 10^{-12}$ dyne/cm^{-2}. Sittler et al. [1987] estimated this magnetic pressure at ~ 7.5 X 10^{-14} dyne/cm^{-2} at a distance ~6000R_J. Therefore we see that magnetic pressure in the magnetosphere should be the primary pressure contributor; however, there was no magnetometer on NH to verify it.

We have demonstrated an example to roughly distinguish heavy and light ion species based on the ratio of count rates from two detectors of SWAP. A laboratory calibration of ground foil has been conducted at SwRI, which may provide additional insight regarding the ion composition in the magnetotail.

We verified that SWAP observed solar wind particles at distance beyond 1650 R_J based on ion characteristics. One of the initial studies of the solar wind and boundary layer beyond 1750 R_J was demonstrated in Section 3.4. In some cases, we were able to identify addition energy peak in the energy spectrogram, and confirmed that the primary and secondary ions are H^+ and He^{++} with the same convection speed. Additional analysis to obtain fluid moments in this region is beyond the scope of this thesis.

The SWAP instrument samples ions with energies below 7.5 keV. In many cases, it only measured low-energy tails of ion distributions. The missing portion of the distribution can be measured by the higher-energy ion instrument, PEPSSI. With data from both instruments, we can better understand the characteristics of ion populations in the magnetotail. The data analysis of PEPSSI is currently conducted at the Johns Hopkins University Applied Physics Laboratory.

REFERENCES

Behannon, K. W., L. F. Burlaga, and N. F. Ness (1981), The Jovian magnetotail and its current sheet, J. Geophys. Res., 86, 8385.

Bhardwaj, A., and G. R. Gladstone (2000), Auroral emissions of the giant planets, Rev. Geophys., 38 (3), 295, doi:10.1029/1998RG000046.

Blanc M, R. Kallenbach, and N.V. Erkaev (2005), Solar System Magnetospheres in The Outer Planets and their Moons, edited by Encrenaz, T., R. Kallenbach, T. Owen, and C. Sotin, Springer, p255

Brown D., M Buckley, M Martinez, (2007), New Horizons − The first mission to Pluto and the Kuiper Belt: Exploring frontier worlds, Jupiter Fly Press Kit, http://www.nasa.gov/pdf/168024main_011607_JupiterPressKit.pdf

Brown D., M Buckley, M Martinez, G. Diller, J Andrews, F Slimmer, (2005), New Horizons − The first mission to Pluto and the Kuiper Belt: Exploring frontier worlds, Launch Press Kit, http://www.nasa.gov/pdf/139889main_PressKit12_05.pdf

Cheng A.F., H.A. Weaver, S.J. Conard, M.F. Morgan, O. Barnouin-Jha,·J.D. Boldt, K.A. Cooper, E.H. Darlington, M.P. Grey, J.R. Hayes, K.E. Kosakowsk, T. Magee, E. Rossano, D. Sampath, C. Schlemm, H.W. Taylor, (2008), Long-Range Reconnaissance Imager on New Horizons, Space Sci Rev, 140, p189-215, doi 10.1007/s11214-007-9271-6

Cooper, J. F., R. E. Johnson, B. H. Mauk, H. B. Garret and N. Gehrels (2001), Energetic Ion and electron of irradiation of the icy Galilean satellites, Icarus 149, 133.

Fountain, G. H., D. Y. Kusnierkiewicz, C. B. Hersman, T. S. Herder, T. B. Coughlin, W. C. Gibson, D. A. Clancy, C. C. DeBoy, T. A. Hill, J. D. Kinnison, D. S. Mehoke, G. K. Ottman,

G. D. Rogers, S. A. Stern, J. M. Stratton, S. R. Vernon, S. P. Williams (2008), The New Horizons spacecraft , Space Sci. Rev., 104, 23, doi: 10.1007/s11214-008-9374-8.

Gierasch, P. J., and P. D. Nicholson (2004), Jupiter, World Book Online Reference Center, World Book, Inc. (http://www.worldbookonline.com/wb/Article?id=ar293080)

Goldstein, M. L., R. P. Lepping, and E. C. Sittler, Jr. (1985), Magnetic field properties of Jupiter's tail at distances from 80 to 7500 Jovian radii, J. Geophy. Res., 90, A9, 8223.

Grzedzielski, S., W. Macek, P. Oberc (1981), Expected immersion of Saturn's magnetosphere in the Jovian magnetotail, Nature, 292, 5824, 615.

Grzedzielski, S., and W. Macek (1984), Comment on the Observed Plasma Densities in Jupiter's Distant Magnetotail (Wake)' A Possible Explanation, J. Geophys Res., 89, A4, 2369.

Guo Y. and Robert W. Farquhar, (2008), New Horizons Mission Design, Space Sci Rev, 140, p49–74, doi 10.1007/s11214-007-9242-y

Hill, T. W., A. J. Dessler and C. K. Goertz (1983), Magnetospheric models, in Physics of the Jovian Magnetosphere, A. J. Dessler (ed.), Cambridge University Press, pp.153-194.

Horanyi M., V. Hoxie, D. James, A. Poppe, C. Bryant, B. Grogan, B. Lamprecht, J. Mack · F., Bagenal, S. Batiste, N. Bunch, T. Chanthawanich, F. Christensen, M. Colgan, T. Dunn, G. Drake, A. Fernandez, T. Finley, G. Holland, A. Jenkins, C. Krauss, E. Krauss, O. Krauss, M. Lankton, C. Mitchell, M. Neeland, T. Reese, K. Rash, G. Tate, C. Vaudrin, J. Westfall, (2008), The Student Dust Counter on the New Horizons Mission, Space Sci Rev, 140, p387–402, doi 10.1007/s11214-007-9250-y

Khurana, K. K., M. G. Kivelson, V. M. Vasyliunas, N. Krupp, J. Woch, A. Lagg, B. H. Mauk, and W. S. Kurth (2004), The configuration of Jupiter's magnetosphere, in Jupiter: The Planet, Satellites and Magnetosphere edited by F. Bagenal, T. E. Dowling, W. B. McKinnon, Cambridge University Press, p.593.

Krupp, N.; V. M. Vasyliunas, J. Woch, A. Lagg, K. K. Khurana, M. G. Kivelson, B. H. Mauk, E. C. Roelof, D. J. Williams, S. M. Krimigis, W. S. Kurth, L. A. Frank, W. R. Paterson (2004a), Dynamics of the Jovian magnetosphere, in *Jupiter: The Planet, Satellites and Magnetosphere,* edited by F. Bagenal, T. E. Dowling, W. B. McKinnon, W.B., Cambridge University Press, p617.

Krupp N., J. Woch, A. Lagg, S. Livi, D. G. Mitchell, S. M. Krimigis, M. K. Dougherty, P. G. Hanlon, T. P. Armstrong, and S. A. Espinosa (2004b), Energetic particle observations in the vicinity of Jupiter: Cassini MIMI//LEMMS results, J. Geophys. Res., 109, A09S10, doi: 10.1029/2003JA010111.

Kurth W. S., J. D. Sullivan, D. A. Gurnett, F. L. Scarf, H. S. Bridge, and E. C. Sittler, Jr. (1982), Observations of Jupiter's distant magnetotail and wake, J. Geophys. Res., 87, A12, 10,373.

Lepping R. P., L. F. Burlaga, M.D. Desch, L. W. Klein (1982), Evidence for a distant (> 8,700 R_J) Jovian magnetotail: Voyager 2 observations, Geophys. Res. Lett., 9, 885.

Lepping, R. P., L. F. Burlaga, L. W. Klein, J. M. Jessena, and C. C. Goodrich (1981), Observations of the magnetic field and plasma flow in Jupiter's magnetosheath, J. Geophys. Res., 86, 8148.

Lewis J. S (1997), The Major Planets in *Physics and Chemistry of the Solar System,* Academic Press, p200.

McComas D., F. Allegrini, F. Bagenal, P. Casey, P. Delamere, D. Demkee, G. Dunn, H. Elliott, J. Hanley, K. Johnson, J. Langle, G. Miller, S. Pope, M. Reno, B. Rodriguez, N. Schwadron, P. Valek, S. Weidner, (2008), The SolarWind Around Pluto (SWAP) Instrument Aboard New Horizons, Space Sci Rev, 140, p261–313, doi 10.1007/s11214-007-9205-3

McComas, D. J., F. Allegrini, F. Bagenal, F. Crary, R. W. Ebert, H. Elliott, A. Stern, P. Valek (2007), Diverse Plasma Populations and Structures in Jupiter’s Magnetotail, Science, 318, 217.

McNutt Jr. R.L., Stefano A. Livi, Reid S. Gurnee, Matthew E. Hill, Kim A. Cooper, G. Bruce Andrews, Edwin P. Keath, Stamatios M. Krimigis, Donald G. Mitchell, Barry Tossman, Fran Bagenal, John D. Boldt, Walter Bradley, William S. Devereux, George C. Ho, Stephen E. Jaskulek, ThomasW. LeFevere, Horace Malcom, Geoffrey A. Marcus, John R. Hayes, G. Ty Moore, Mark E. Perry, Bruce D. Williams, Paul Wilson IV, Lawrence E. Brown Martha, B. Kusterer, Jon D. Vandegriff, (2008), The Pluto Energetic Particle Spectrometer Science Investigation (PEPSSI) on the New Horizons Mission, Space Sci Rev, 140, p315–385, doi 10.1007/s11214-008-9436-y

Ness, N. F., M. H. Acufia, R. P. Lepping, L. F. Burlaga, K. W. Behannon, and F. M. Neubauer (1979a), Magnetic field studies at Jupiter by Voyager 1: Preliminary results, Science, 204, 4396, 982.

Ness, N. F., M. H. Acufia, R. P. Lepping, K. W. Behannon, L. F. Burlaga, and F. M. Neubauer (1979b), Jupiter's magnetic field, Nature, 280, 799.

Ness, N. F., M. H. Acufia, R. P. Lepping, L. F. Burlaga, K. W. Behannon, and F. M. Neubauer (1979c), Magnetic field studies at Jupiter by Voyager 2: Preliminary results, Science, 206, 4421, 966.

Reuter, D. C., S. A. Stern, J. Scherrer, D. E. Jennings, J. W. Baer, J. Hanley, L. Hardaway, A. Lunsford, S. McMuldroch, J. Moore, C. Olkin, R. Parizek, H. Reitsma, D. Sabatke, J. Spencer, J. Stone, H. Throop, J. V. Cleve, G. E. Weigle, L. A. Young, Ralph: A vsible/infrared imager for the New Horizons Pluto/Kuiper Belt Mission, Space Sci. Rev., 140, 129, doi: 10.1007/s11214-008-9375-7.

Russell, C. T. (2001), The dynamics of planetary magnetospheres, Planetary and Space Science, 49, 1005, doi:10.1016/S0032-0633(01)0017-4.

Russell, C. T. (1993), Planetary magnetospheres, *Reports on Progress in Physiscs* , 56, 687, doi: 10.1088/0034-4885/56/6/001.

Scarf, F.L. (1979), Possible traversals of Jupiter's distant magnetic tail by Voyager and by Saturn, J. Geophys. Res., 84, 4422.

Sittler, Jr., E. C., R. P. Lepping, B. H. Mauk, and S. M. Krimigis (1987), Detection of a hot plasma component within the core regions of Jupiter's distant magnetotail, J. Geophys. Res., 92, A9, 9943.

Space Study Board (1994), An Integrated Strategy for Planetary Sciences 1995-2010 National Research Council, National Academy Press, Washington, D. C.

Stern, S. A. (2008), The New Horizons Pluto Kuiper Belt mission: An overview with historical context, Space Sci. Rev., 140, 3, doi:10.1007/s11214-007-9295-y.

Stern, S. A., D. C. Slater, J. Scherrer, J. Stone, G. Dirks, M. Versteeg, M. Davis, G. R. Gladstone , J. W. Parker, L. A. Young, O. H.W. Siegmund (2008), ALICE: The ultraviolet imaging spectrograph aboard the New Horizons Pluto–Kuiper Belt mission, Space Sci. Rev., 140, 155, doi: 10.1007/s11214-008-9407-3.

Tyler, G. L., I. R. Linscott, M. K. Bird, D. P. Hinson, D. F. Strobel, M. Pätzold, M. E. Summers, K. Sivaramakrishnan (2008), The New Horizons radio science experiment (REX), Space Sci. Rev., 140, 217, doi: 10.1007/s11214-007-9302-3.

Weaver, H. A., W. C. Gibson, M. B. Tapley, L. A. Young, and S. A. Stern (2008), Overview of the New Horizons science payload, Space Sci. Rev., 140, 75, doi: 10.1007/s11214-008-9376-6.

Woch J., N. Krupp, A. Lagg, B. Wilken, and S. Liviand D. J. Williams (1998), Quasi-periodic modulations of the Jovian magnetotail, Geophys. Res Lett., 25, 8, 1253.

BIOGRAPHICAL INFORMATION

Debrup Hui received his MS in Elcetronic Sciecne from University of Calcutta, Kolkata, India in the year 2003. After working at Saha Institute of Nuclear Physics (SINP) for a brief period of time on Nuclear Instrumentation, he joined S.K. Mitra Center for Research in Space Environment to work in an Indian Space Research Organization (ISRO) project named “Space Weather”. In 2006, he became a project fellow at the Center for Advanced Studies at the Institute of Radiophysics and Electronics, University of Calcutta. In May, 2007 he again joined S.K. Mitra Center for Research in Space Environment as a research fellow until he joined UT Arlington as a graduate student. His interest fields are Space Science and Technology which includes planetary magnetospheres, MI coupling, Ionospheric anomalies, GPS positioning systems, satellite instrumentation and communication. He enjoys working with instruments and at the same time extracting science from it.